Università degli Studi di Ferrara
Dottorato di Ricerca in Fisica, XXIV Ciclo
Coordinatore Prof. Filippo Frontera

Proton induced Deuteron Breakup reaction studies at COSY

Dottorando
Susanna Bertelli

Tutore
Dr. Paolo Lenisa

Anni 2009-2011

Abstract

The present thesis is dedicated to the study of the *pd* Breakup reaction. The study is part of a project, realized at the COSY storage ring, finalized to map pd breakup spin observables in a kinematical region where measurements are limited altough strongly necessary to fix important constraints for investigating the role of the three-nucleon forces via the Chiral Perturbation Theory.
In the first part of the work, I developed an analysis chain to determine whether a detection system based on Silicon Tracking Telescope, originally conceived to identify *pd* elastic events, was capable to identify the products of the *pd* Breakup reaction. This feasibility study has been successfully applied to an existing data sample taken at the COSY ring in Febrauary 2008, with a vertically polarized proton beam of 49.3 MeV kinetic energy impinging on a Deuterium cluster target. In a following phase, the identified *pd* Breakup events have been employed to tune an algorithm to measure the analysing power in *pd* Breakup reaction using the neutron asymmetries. This observable represents one of the probes to constrain Chiral Perturbation Theory. The analysis of the available data sample has allowed to outline the experimental conditions required for an exhaustive investigation of the spin observables in *pd* breakup reaction. On the other side, the low statistics and the not optimal working conditions of the detection system made not possible to finalize the result on the existing data sample. At present the developed analysis is being exploited on a new sample of data acquired during 2011 beam-time.
In parallel, I carried out a study of a new apparatus devoted to the *pd* Breakup investigation. In particular double spin asymmetries in *pd* Breakup offer a rich laboratory where to test Chiral Perturbation Theory. For accessing these observables, an experiment where both the proton beam and the deuterium target are polarized would be re-

quired. In addition a detection system providing a large azimuthal and longitudinal phase-space coverage would be needed.
For this reason, I implemented the analysis software, developed in the first stage of my work, for the characterization and the optimization of this dedicated detection system on the basis of Monte Carlo generated data. The results of the analysis served as a guidance for the detector design and have been included in a proposal[1] submitted and successfully reviewed from the PAC of COSY.

Riassunto

Questo lavoro di tesi è dedicato allo studio della reazione di frammentazione del Deutone indotta da un fascio di protoni, *pd* Breakup. Questo studio costituisce parte di un progetto di ricerca, realizzato presso l'anello di accumulazione COSY, finalizzato alla misura delle osservabili di polarizzazione della reazione di *pd* Breakup, in una regione cinematica in cui le misure esistenti sono limitate sebbene indispensabili per fissare vincoli utili per investigare il ruolo delle forze che agiscono tra tre nucleoni 3NF attraverso la Chiral Perturbation Theory.
Nella prima parte del lavoro, ho sviluppato una catena di analisi per stabilire se un sistema di rivelazione basato su sensori di silicio, concepiti originariamente per identificare gli eventi del canale *pd* elastico, fosse in grado di identificare anche i prodotti della reazione di *pd* breakup.
Questo studio di fattibilità è stato applicato con successo ad un campione di dati acquisiti presso l'acceleratore COSY nel Febbraio 2008, in cui sono state indotte collisioni tra un fascio di protoni polarizzato ad un'energia cinetica di 49.3 MeV e un bersaglio di Deuterio. Nella fase successiva, gli eventi di *pd* Breakup identificati sono stati utilizzati per mettere a punto un algoritmo per determinare l'analysing power della reazione di *pd* Breakup usando le asimmetrie del neutrone. Questa osservabile rappresenta un test chiave per vincolare la Chiral Perturbation Theory. L'analisi del campione di dati a disposizione ha consentito di delineare le condizioni sperimentali ideali per studiare in maniera esaustiva le osservabili di polarizzazione della reazione *pd* Breakup. Tuttavia a causa della statistica limitata e delle condizioni di lavoro non ottimali del sistema di rivelazione, non è stato possibile finalizzare un risultato per il campione di dati esistente. Al momento la catena di analisi sviluppata viene impiegata per studiare un nuovo

campione di dati acquisiti durante una presa dati nel 2011.
In parallelo, ho sviluppato l'analisi di un nuovo apparato esplicitamente dedicato allo studio del canale *pd* Breakup. Le *double spin asymmetries* nel canale di *pd* Breakup costituiscono un ricco laboratorio dove testare la Chiral Perturbation Theory. Per accedere a queste osservabili, è necessario realizzare un esperimento in cui il fascio di protoni e il bersaglio di Deuterio siano entrambi polarizzati e il sistema di rivelazione sia caratterizzato da una estesa copertura longitudinale e azimutale dello spazio delle fasi.
A questo scopo, ho implementato il software di analisi sviluppato per la prima parte del lavoro di tesi, al fine di caratterizzare e ottimizzare il sistema di rivelazione dedicato utilizzando dati Monte Carlo. I risultati di questa analisi sono serviti come guida per il design del sistema di rivelazione e sono stati inclusi in un proposal[1] che è stato sottomesso e approvato con successo dal PAC di COSY.

Contents

Abstract **iii**

Riassunto **v**

Introduction **3**

1 Physics Motivation **7**
1.1 Conventional approaches to the Nuclear Force problem 8
1.2 The Chiral Perturbation Theory 10

2 Experimental Setup **15**
2.1 The *COSY* facility 15
2.1.1 Electron Cooler 17
2.2 PAX beam polarimeter 17
2.2.1 Deuterium cluster target 17
2.2.2 SILICON TRACKING TELESCOPES 19
2.2.3 Front-end electronics 20
2.2.4 Geometry and Trigger 21

3 Deuteron Breakup events analysis **25**
3.1 *pd* Breakup vs *pd* elastic 26
3.1.1 Kinematics of $pd \to ppn$ 27
3.2 Simulations and Data 28
3.2.1 RUN SELECTION 29
3.3 Track Reconstruction 30
3.3.1 Particle Identification 32

3.3.2 Track "1" reconstruction 34
3.3.3 Track "2" reconstruction 34
3.3.4 Third layer Calibration 35
3.3.5 Track "3" reconstruction 36
3.4 Deuteron Breakup samples 38
3.5 Efficiency of Breakup identification 40
3.6 Phase Space Coverage 42
3.7 Method development for the analysing power A_y in pd→ppn 49
3.7.1 Considerations 53

4 Future plans: Dedicated setup for *pd* Breakup studies 55
4.1 PAX Experimental Setup 55
4.1.1 The COSY beam 56
4.1.2 Polarized Internal Target 57
4.2 PAX Multipurpose Detection System 59
4.3 *pd* Breakup event generation 61
4.4 *pd* Breakup events identification 61
4.4.1 Stopped protons: track "1" 63
4.4.2 Stopped protons: track "2" and "3" 63
4.5 *pd* Breakup reconstruction efficiency 65
4.6 Phase space coverage 67
4.6.1 Considerations 70

Conclusions 71

Appendix A 73

Appendix B 79

Acknowledgements 87

Introduction

One of the main issues in nuclear physics is determining the nature of the interactions between the nucleons which is crucial for investigating the properties of nuclei. In general observables at the energy relevant to nuclear physics are well described by a nucleon-nucleon (NN) potential. Altough much has been learned about the NN interaction, it is of interest to find out whether these forces can also be involved in systems where more than two nucleons interact.
In a three-nucleon system it is important to investigate how the interaction between two nucleons is influenced by the presence of a third nucleon. This extra effect is related to a force which is beyond the two-nucleon interaction and is known as three-nucleon force (3NF).
At present, few-nucleon systems can be studied using phenomenological models that, despite some remarkable successes in describing experimental data, leave some open problems, among which is the loose connection to QCD.
The drawbacks of phenomenological models are overcome by employing the modern theory of nuclear force Chiral Perturbation Theory (ChPT). ChPT is an effective field theory (EFT), that allows a systematic approach to studying low-energy hadron dynamics adhering to the symmetries of QCD.
To provide a better understanding of 3NFs effects, differential cross sections and polarization observables have been measured in nucleon-deuteron scattering. In a three-nucleon (3N) continuum the experimental data and the theoretical predictions reveal both very good agreement and significant disagreement.
An alternative to Nd scattering, spin observables in $pd \to ppn$ deuteron breakup reactions, due to the richer kinematics, offer a fertile laboratory where studying the 3NFs.
In order to achieve a conclusive experimental description of three-

nucleon interactions and in particular their spin dependence, a majority of possible observables need to be measured with high accuracy, since 3NFs effects are in general very small in the three-nucleon system. In particular the energy range between 30 and 50 MeV is an ideal range where the 3NF effects are expected to appear and be significant and at the same time it is a suitable range to test the predictive power of chiral EFT. In this range previous measurements are scarce and limited and it would be very interesting to have at disposal a complete database.
The reaserch of this thesis has been performed in the framework of the PAX Collaboration that aims at the production of the first polarized antiproton beam. In particular, in the past three years, the PAX Collaboration has performed a series of tests on protons at COSY aimed at investigating spin-filtering and spin-flip as possible mechanisms to polarize a stored beam of protons. In this environment a dedicated polarimeter to measure the stored beam polarization has been installed in the COSY ring. The polarimeter has been implemented by means of a couple of Silicon-Tracking Telescopes that serve to detect deuterons coming from *pd* elastic scattering.
The first part of my work has been devoted to a feasibility study of the use of the same polarimeter to identify deuteron breakup events, which constituted part of the background with respect to the elastic scattering. To this purpose, I analyzed the data taken during a dedicated beamtime in 2008 and I developed a chain of selection criteria to carry out the *pd* Breakup events identification. After a clean identification of the deuteron breakup events, I investigated the possibility to access the neutron analyzing power by the two outgoing protons detected in the polarimeter.
This analysis procedure of *pd* breakup events forms part of the feasibility studies for an accepted experiment proposal submitted by the PAX collaboration [1] to be performed at COSY. The objective of the planned experiment is to provide a means of testing the predictive power of chiral EFT, including the effects of three-nucleon forces in few-nucleon systems. Most of the spin correlation parameters and the vector and tensor analysing powers in *pd* breakup reactions at 30-50 MeV proton beam energy will be measured with large phase space coverage.
To this aim a dedicated detection system is being developed that will also serve as polarimeter for the other planned experimental activities

at the newly installed PAX setup at COSY. This detector development was the object of the second part of my thesis. In particular I analyzed Monte Carlo data for the characterization and the optimization of this detection system. The results of the simulation analysis were adopted in the proposal[1].
The thesis is organized as follows: Chapter 1 reports the motivations supporting the necessity of additional measurements in the three nucleon sector; in Chapter 2 the experimental setup used to realize the feasibility study for pd-breakup is presented; Chapter 3 is devoted to the procedure of breakup identification and analysis; in Chapter 4 the results of Monte Carlo studies for the future dedicated detector are shown.

Chapter 1

Physics Motivation

One of the main issues in Nuclear Physics is the role of the forces acting between nuclear constituents and few-nucleon systems represent the ideal laboratories where these forces can be investigated. In particular it is important to study the dynamics related to the presence of a third nucleon, which is crucial to understand the contributions of three-nucleon forces (3NFs).
Even if the theory of 3NFs was developed in the 30's of the last century [2], still many problems remain open. Presently, the spin structure of the three-nucleon continuum exhibits disparate results when comparing experimental data to theoretical predictions based on two-nucleon potentials either with or without the inclusion of three-nucleon interactions. A detailed review of the current status of the research on the role of the three-nucleon forces can be found in [3]. The rich kinematical region in proton-deuteron breakup reactions at low to intermediate energy offers a good testing ground for the chiral effective field theory (EFT), the modern theory of nuclear forces in the low-energy regime. In particular, in the energy range between 30 and 50 MeV, that is of interest for the experiments presented in this thesis, very scarce polarized experimental data exist. This is an ideal range where the predictive power of chiral EFT in three-nucleon continuum can be tested by measuring analysing powers and double spin observables with high precision over large areas of the phase-space.
The chapter is organized as follow: section 1 introduces a survey of the main approaches developed to study the contribution of the three-nucleon forces (3NFs) in nuclear systems, section 2 provides a review on how nuclear forces emerge from low-energy QCD via EFT.

1.1 Conventional approaches to the Nuclear Force problem

Since the typical energy scale in Nuclear Physics is in the order of nuclear binding energies, the N-body problem can be described by the non-relativistic Schrödinger equation. In a first approximation, observables in this energy range are well described by a nucleon-nucleon (NN) potential. The conventional way to describe the nuclear force is

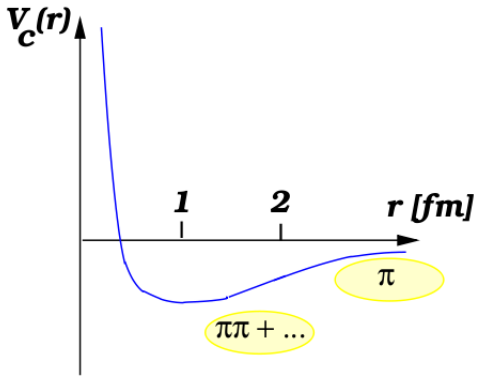

Figure 1.1: The central nucleon-nucleon (NN) potential is displayed. The longest range contribution corresponds to the 1-π exchange, the intermediate range attraction is described by 2-π exchanges and other shorter range contributions. At shorter distances, the NN interaction is strongly repulsive. This figure is taken from Ref. [4].

based on the meson-exchange picture as proposed by Yukawa[5]. This approach enriched by meson field theory and dispersion relations (employed to construct the two-pion exchange contribution) brought to the development of high precision semi-phenomenological nucleon-nucleon (NN) potential models like AV18[6], CDBonn[7, 8, 9], Nijmegen I and II[10]. These models describe the long-range tail of the nuclear force due to electromagnetic interaction and the one-pion exchange potential and parametrize the medium- and short-range contributions. These potentials can reproduce a large sample of proton-proton and neutron-proton scattering data oberservables up to the pion production threshold with a χ^2/datum $\sim$1 and provide an accurate representation of most deuteron properties. In Nd scattering differential cross section, analysing powers and spin-transfer coefficients are well described at low incident beam energy using solely two-nucleon forces (2NFs), but

a discrepancy with data is observed as the energy increases (for the analysing power this discrepancy is known as A_y-puzzle[11]).
The difference between calculations including solely 2NFs and data is usually interpreted as an indication of the existence of three-nucleon forces (3NFs). 3NFs are many-body interactions that have to be included beyond pair forces to describe nuclei and nuclear reactions properly. Systematic studies of the dynamics of systems involving three or four nucleons allow precise tests of the role and the structure of the 3NFs.
The Urbana-Argonne group[12] showed that three-nucleon forces have to be included to describe the nuclear binding energies which are known to be underestimated by two-nucleon potentials.
The extension of Yukawa theory to 3NF is due to Fujita and Miyazawa[13], who implemented the meson exchange idea by sandwiching the pion-nucleon scattering amplitude between nucleon lines, thus originating the 3NF of longest range.
The described approach is frequently used in nuclear structure and reaction calculations but reveals some deficiencies like the absence of a way to assign a theoretical error, the difficulty to implement gauge and chiral symmetries, the inconsistency between three-nucleon forces and the nucleon-nucleon interaction models and a very loose connection to Quantum Chromo Dynamics (QCD).
These deficiencies can be overcome in chiral Effective Field Theory (EFT), an approach to study the low-energy hadron consistent with the QCD. Chiral EFT is linked to QCD via its symmetries and allows to treat the low-energy properties of hadronic systems in a controlled way. When this method is applied to a system of three nucleons, graphs including 3NFs appear naturally in a complete agreement with the chiral NN interactions, as described in the next section.
The experimental data and the theoretical predictions for reactions including three nucleons at low and intermediate energies are today at variance. In some parts of the phase space for some observables, the inclusion of the 3NF in the models lead to a good agreement between data and theory, while in other parts the agreement is worsened[14, 15, 16]. This ambiguity requires a complete and high precision database.
The Deuteron breakup offers, with respect to the elastic channel, a richer kinematics to study observables in the three nucleon continuum that is crucial to investigate the structure of the nuclear force and to

demonstrate the possibile evidence of the 3NFs.

1.2 The Chiral Perturbation Theory

Chiral Perturbation Theory (ChPT) is the effective theory of Quantum ChromoDynamics (QCD) formulated by Weinberg[17] and developed into a systematic tool for studying the properties of hadronic systems at low energies in a model-independent framework. It is based on the spontaneously broken chiral symmetry of QCD, providing a method to improve the results by considering higher orders in a perturbative expansion. Weinberg attempted a generalization of this method to the few-nucleon sector, facing a non-perturbative problem since one has to deal with the strong nucleon-nucleon interaction.
In the framework of ChPT two kind of interactions emerge: long-range pion exchanges and contact interactions, with the associated low-energy constants (LEC). Due to chiral symmetry, a power counting can be used to estimate the contribution of individual graphs to the NN interaction. Weinberg proposed to apply chiral perturbation theory to the effective potential, defined as the sum of all the contributions of irreducible diagrams, instead of applying it to the scattering amplitude, obtained by solving the corrisponding dynamical equation. In this way, only a finite number of diagrams contributes at a given order and the nonperturbativity of nuclear systems is taken into account.
In this framework, one can consider the most general effective Lagrangian L_{EFF} for pions and nucleons consistent with the symmetries of QCD. Nuclear forces can be determined from L_{EFF} perturbatively via an expansion in powers of Q/Λ, where Q refers to a typical momentum of the nucleons or the pion mass and Λ is the chiral symmetry-breaking scale of ≈ 1 GeV.
The importance of a particular contribution to the nuclear potential is fixed by the power ν of the expansion parameter Q/Λ, providing the accuracy at order ν. In this sense, the theory can be calculated at any accuracy and has a predictive power. The nuclear force can be espressed by:

$$V = \sum_{\nu} V^{\nu} = V^0 + V^1 + V^2 + ... \tag{1.1}$$

The structure of the nuclear force at lowest orders of the chiral expansion is shown in Fig.1.2.

Chiral power counting explains the dominance of the 2NF contribution that starts at ν=0.

- ν=0: at this leading order (LO), the 2NF is provided two nucleon-nucleon contact interactions without derivates, represented in Fig.1.2 by the four-nucleon-leg graph with a small-dot vertex, and by one pion exchange, second diagram in the first row of Fig.1.2. The coupling costants linked to NN contact interation at this and higher orders can be derived from the low-energy nucleon-nucleon data.

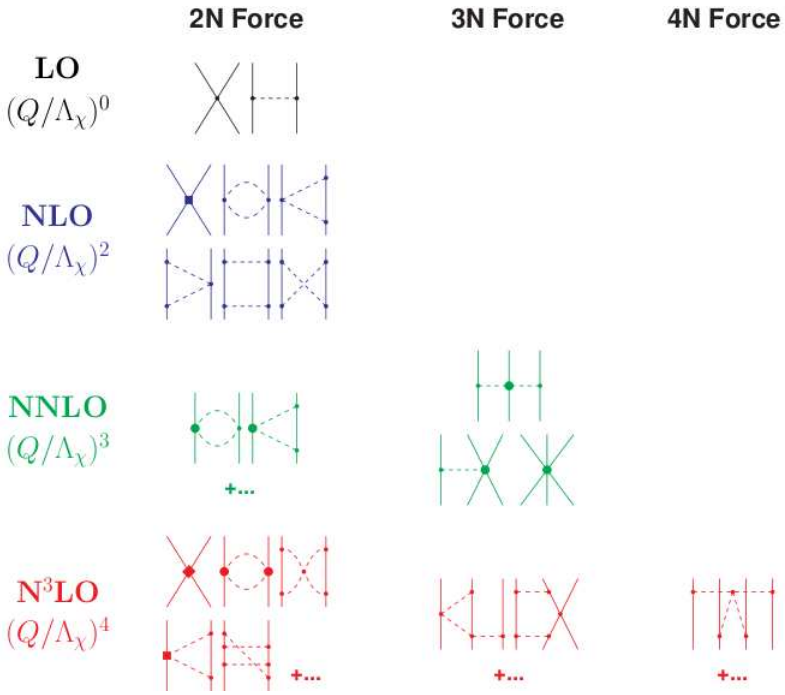

Figure 1.2: The Hierarchy of nuclear forces in ChPT is shown. Solid lines are nucleons and dashed lines are pions. Solid dots, filled/open squares and circles depict vertices from L_{EFF}. Figure taken from ref.[4].

- ν=1: The parity conservation precludes any contributions at this order.

- ν=2: The first corrections at next-to-leading order (NLO) arise from two-pion exchange, without new parameters and contact interactions quadratic in the momenta or pion mass.

- ν=3: at next-to-next-to-leading order (N^2L0), two-pion exchange contributions together with one insertion of the subleading $\pi\pi$NN vertices has to be considered. The related low-energy constants $c_{1,3,4}$ are determined by πN scattering. At this level the first contribution to the 3NF from diagrams appears[18]. Two-pion exchange part involves no new parameters, whereas the two other topologies depend on one unknown constant each, which can be fixed from three- or more-nucleon observables.

- ν=4: at next-to-next-to-next-to-leading order (N^3LO), further corrections to the 2NF has to be included, considering the subleading two-pion exchange, the leading three-pion exchange terms and the connected contact terms; at this order the four-nucleon force (4NF) originates.

In the framework of EFT it is natural to define a qualitative explanation of the observed hierarchy of two-, three-, more-nucleon forces: $V_{2N} \gg V_{3N} \gg V_{4N}$.
By far, the 2NF has been worked out and applied to N^3LO in the NN system, while the results for three- or more-nucleon systems are available up to N^2LO[19].
The Low Energy Constants (LECs) D and E entering the expression of 3NF are determined by fitting the ^{3}H and ^{4}He binding energy[20] and either the nd scattering lenght[21] or the properties of the nuclei[22]. Once D and E are fixed, the resulting nuclear Hamiltonian can be employed to describe the dynamics of few-nucleon systems. This method has the advantage, with respect to the other approaches, of estimating uncertainties of the obtained predictions.
3N scattering observables and in particular the breakup reaction is a fertile testing ground for the chiral forces. The deuteron breakup reaction has been recently measured at the intermediate energy of E_N=65 MeV (E_N refers to kinetic energy of the incident nucleon beam) and some data, concerning cross sections, in kinematical configurations as the final state interaction, symmetric space star and quasi-free scattering[1] are available in the range below 20 MeV.
No systematic data exist in the energy range between 30 and 50 MeV. This energy range is extremely suitable to find relevant contributions

[1] In the final state interaction FSI, two nucleons leave the interaction region with equal momenta; in the symmetric star configuration, the three nucleons have equal energies; in the quasi-free scattering, one nucleon in the final state is at rest in the laboratoty system

due to 3NF and at the same time the energies are low enough to offer precise theoretical predictions based on chiral EFT. Data in this energy range will provide an independent source for a determination of the LECs D and E and thus will allow a consistency check of the theoretical approach. Moreover, precise data in this range will be relevant to explore effects of the new structures which appear in the 3NF at N^3LO without any additional unknown parameters. This is the energy range where the planned *pd* breakup double-polarized experiment will take place at the COSY-facility, see the beam proposal submitted to the COSY Program Advisory Program[1]. To map out 3N, precision measurements of some relevant observables as well as a large phase space coverage are required; these conditions are fulfilled using both polarized beam and target and a large azimuthal coverage detection system. Appendix A is devoted to the description of the analysis tool *Sampling method*, that provides a direct comparison between experiment and theory and will be applied for the future measurements. In particular the spin observables that can be accessed in a double polarized *pd* breakup experiment are reported. In Chapter 4 the future dedicated *pd* breakup experimental setup is described.

Chapter 2

Experimental Setup

The experimental data analyzed in this thesis have been taken in a fixed-target experiment performed at the COoler SYnchrotron COSY of the Forschungszentrum Julich (FZJ). In these experiments a vertically polarized proton beam of 49 MeV kinetic energy scatters on an unpolarized deuterium target. In the scattering process both *pd* elastic and *pd* breakup events can take place. These two reactions are identified by the Silicon Tracking Telescope (STT) detection system, which is also part of the beam polarimeter. In this chapter a technical overview of the various components of the experimental setup is presented.

2.1 The *COSY* facility

The COoler SYnchroton (COSY) at the Institut for Nuclear Physics (IKP) of the Research Centre of Juelich (FZJ) is an accelarator which provides proton and deuteron beams (Δp/p=10^{-4}-10^{-3}) in the momentum range from 300 MeV/c (550 MeV/c in the deuterons case) up to 3.7 GeV/c. The phase space cooling of the stored beam is provided to an electron cooler (up to a momentum of 600 MeV/c) and completed by a stochastic cooling that covers the momentum range above 1.5 GeV/c. Unpolarized and polarized beams originate from external or internal experiments. Polarized beams are produced by a polarized ion source which provides a vector polarized proton beam and deuteron beams with all possible combinations of vector and tensor polarization. The typical achieved filling (number of particles stored in the accelerator)

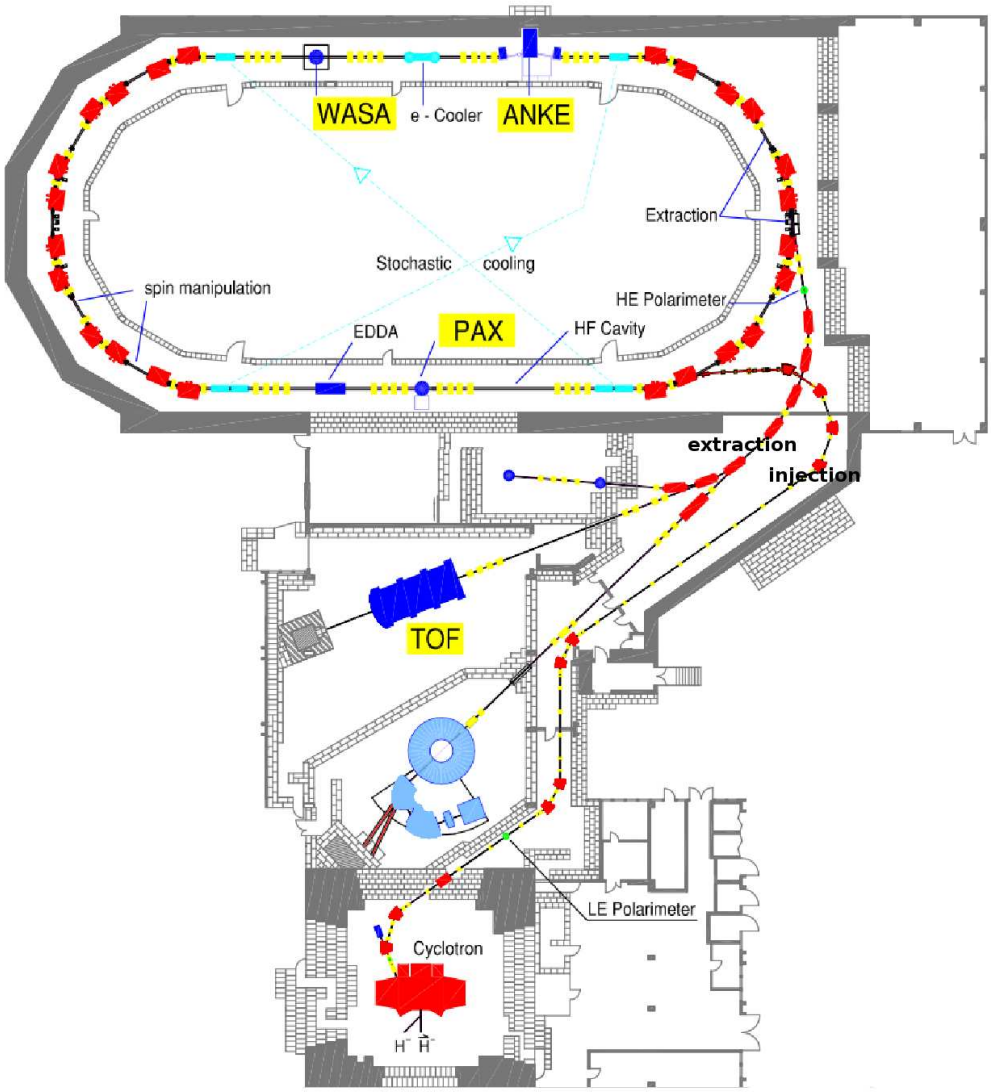

Figure 2.1: The COSY-facility with the injection and extraction line; the main internal and external esperiments are indicated.

for a transversely polarized proton beam is 10^{10} particles ($3 \cdot 10^{10}$ for deuterons) with 70% of polarization (70% vector and 50% tensor polarization for deuterons). An overview of the COSY-ring is shown in Fig.2.1 indicating the main experiments and in particular the target point for the Polarized Antiprotons eXperiments (PAX).

2.1.1 Electron Cooler

The COSY electron cooler has been optimized for electron energies up to 100 keV, enabling phase space cooling up to 183.6 MeV proton energy. Its basic application is reducing the large emittance and the large momentum spread due to the injection stripping process before the ion beam is accelerated to the requested energy[23]. The electron beam is extracted from a thermionic cathode and electrostatically accelerated up to the velocity ion beam. The electron beam is driven by the longitudinal magnetic field provided by toroids and solenoids through the region of interaction with the ion beam and, after energy recovering by electrostatic decelaration, it enters the collector. Two solenoids with reversed longitudinal field up- and downstream of the cooler device hinder coupling between horizontal and vertical phase space plane and distortion of the ion spin direction in the COSY ring. Steerer magnets balance the orbit distortion induced by the toroids and enable the match between the ion beam and the electron beam in position and in angle. When the optimum setting is found, the electron beam can be tilted by steering coils on the drift solenoid and it slightly reduced its cooling force.

2.2 PAX beam polarimeter

The beam polarization is measured using the Silicon Tracking Telescopes (STTs) detection system, placed at the ANKE interaction point, see Fig.2.1. As described in detail in section 3, the beam polarization can be determined exploiting the left-right asymmetry of the selected deuterons from proton-deuteron elastic scattering, where the deuterium is delivered from the ANKE Deuterium cluster target[24].

2.2.1 Deuterium cluster target

A Deuterium cluster target is placed at the internal target position of the ANKE experiment. It provides a target density of 10^{13}-10^{15} atoms/cm^2 and a target beam of 10 mm diameter, entailing a small beam target overlap. Clusters of 10^3-10^4 atoms are delireved from a Laval-nozzle, where pure hydrogen or alternatively deuterium gas is cooled down to a the temperature range of 20-30 K. At the pressure

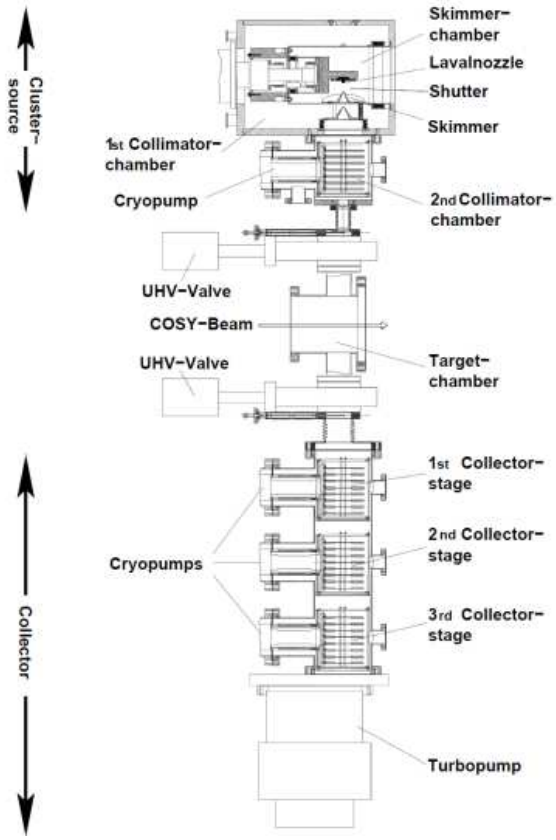

Figure 2.2: A schematic view of the Deuterium Cluster Target is shown. The cluster source placed above the COSY beam provides a well-defined target beam of hydrogen or deuterium clusters. The collector section keeps the vacuum below 10^{-7} mbar.

range of 15-20 bar, the gas is forced into the vacuum of the skimmer chamber using the Laval-nozzle of 20 μm opening diameter. Once inside the skimmer chamber, the gas expands adiabatically and it cools down. In oversaturated gas conditions, the condensation of atoms into clusters takes place. There are about 10^3 atoms close to the triple point per cluster. The skimmer provides the separation of the cluster beam from the residual gas which is the main component of the total gas load into the skimmer chamber. The target section called collector, see Fig.2.2 hosts a differential pumping system (three cryo-pumps plus one turbomolecolar pump) which limits the gas load into the target chamber, keeping the vacuum below 10^{-7} mbar.
After having crossed the accelerator beam, the cluster beam enters the collector stage, placed below the target chamber, see Fig.2.3.

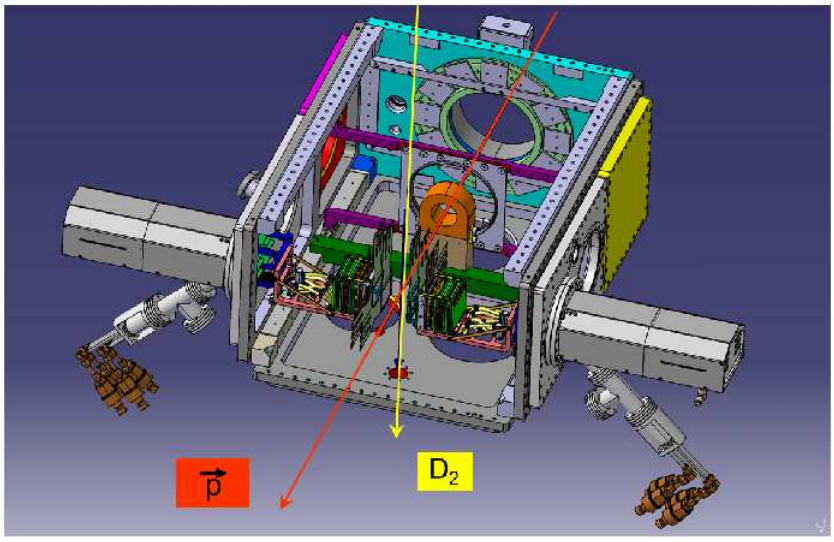

Figure 2.3: The two Silicon Tracking Telescopes placed colse to the beam-target overlap region in the target chamber is shown. The polarized proton beam (red line) enters the chamber and hits the deuterium cluster target (yellow line), injected from the top.

2.2.2 SILICON TRACKING TELESCOPES

The detection system consists of two groups of silicon strip detectors arranged in a telescope layout around the beam target overlap region. A Silicon Tracking Telescope is made by three double-sided microstrip detectors of different thickness; the first layer can be of $65\mu m$ or $300\mu m$ thickness, the second layer of 300 μm thickness and the third layer is a 5100 μm sensor to maximize the number of stopped particles.
This system is able to fullfill the following tasks:

- Identification of stopped particles by the ΔE/E method, providing in particular the proton identification in the kinetic energy range $2.5 - 40$ MeV with a resolution of 150 keV.
- Particle tracking over a large energy range, from 2.5 MeV up to minimum ionizing particles (MIP); vertex resolution of 1 mm.
- Self-triggering capabilities realized by a fast amplifier with a peaking time of 75 ns by means of which a particle passage is registred fast and provide a trigger; in this way the system behaves like a stand-alone detector.
- High rate capability and high modularity.

The particle identification, crucial for the polarization measurement, is realized using the ΔE/E method analysing the correlation between the energy loss in different layers, as described in section 3.
The detectors used for the first two layers of the STTs are the BaBar IV detectors and have been originally designed by the company Micron Ltd [25] for the BaBar experiment [26, 27, 28, 29, 30] at the SLAC PEP-II B factory. The size of their active area is 51mm × 62mm and the strip pitch is of 400 μm.
The p-doped side has 1023 strips, whereas the n-doped side has 631 strips. In order to increase the effective strip pitch up to 400 μm, the strips are arranged into groups that are connected to segments on the kapton flat cable used to connect the detector and the front-end electronics (see Fig.2.4 for the connection scheme).
A vacuum-feedthrough for each segment is not applicable because of the large number of the readout channels, one per segment, so the front-end electronics is used in vacuum.
The thick Lithium drifted Silicon detectors Si(Li)[31] used for the third layer has an active area of 64 mm × 64 mm and a strip pitch of 666 μm (96 strips per side). They have been developed in the detector laboratory of the Institut für Kernphysik (IKP) of FZJ. They allow to stop particles up to an energy of about 32 MeV for protons and 43 MeV for deuterons.

2.2.3 Front-end electronics

The signals coming from the silicon sensors are transported to the in-vacuum front-end electronics by kapton flat cables. The VA32TA2 chips are used. The chip provides a low trigger threshold of 100 keV; two boards 90 mm×90 mm (one per detector side) with 5 chips are utilized. The front-end electronics consists of 32 channels logically separated into an amplitude and a trigger part. In the preamplifier stage, a charge signal in the input pad of the channel is amplified and then split into the two branches. The pre-processed signals are driven by addictional kapton flat cables to the vacuum feedthrough connectors. The connectors are placed on the electronics to favour the dismounting of the kapton flat cables in order to fulfill the modularity request.
A single front-end electronics board is controlled outside of the vacuum via one interface card which provides power supplies, control signals,

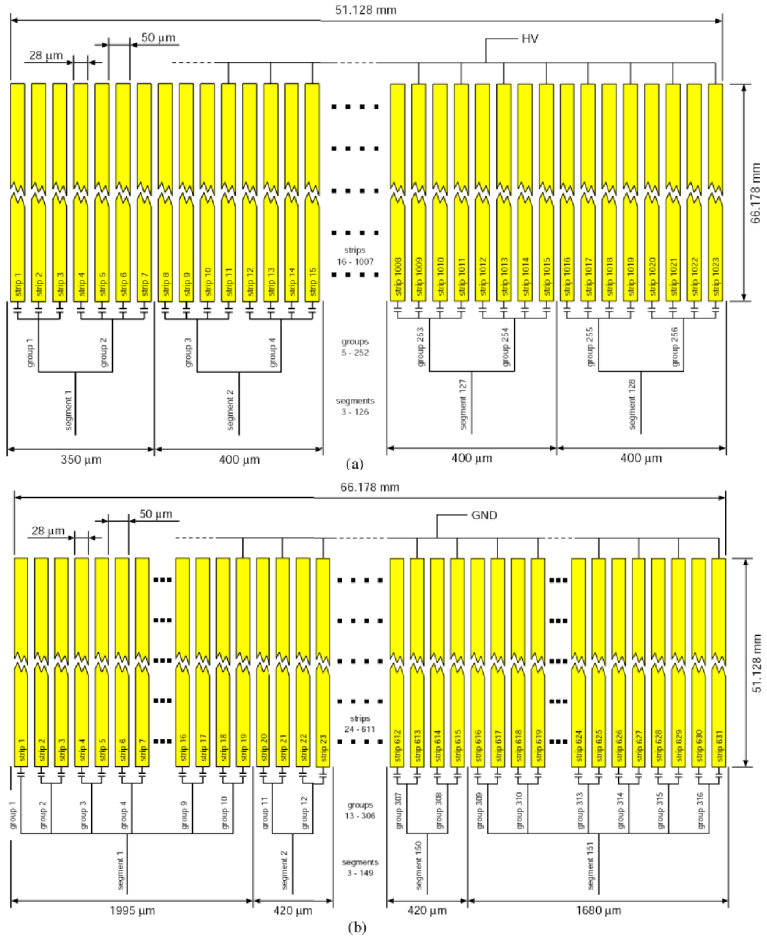

Figure 2.4: The connection scheme of the p-doped side (a) and n-doped side (b) of the BaBar IV detector.

trigger pattern threshold and calibration pulse amplitudes. The total read-out chain contributes to a total dead time of less than 50 μs.

2.2.4 Geometry and Trigger

The displacement of the STTs has been optimized to measure the beam polarization in proton-deuteron elastic collisions according to Monte Carlo simulations.
The geometry of the setup has to meet these requirements:

- the beam polarization has to be measured with a small statistical error.

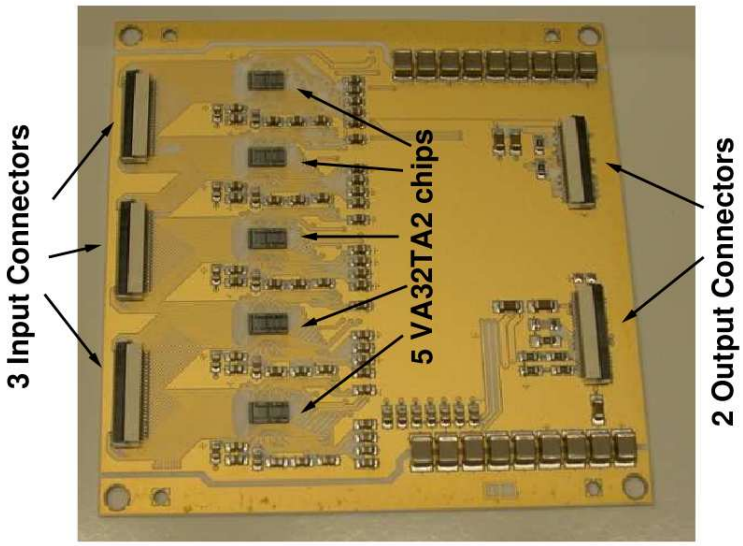

Figure 2.5: The in-vacuum front-end electronic board is shown, with the input/output connectors and the front-end chips indicated.

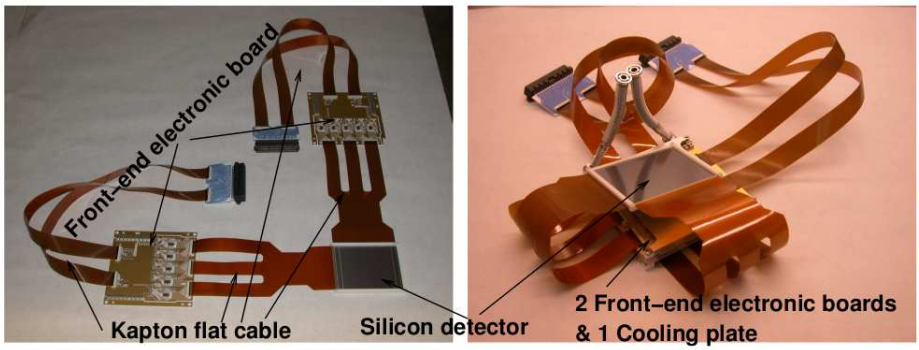

Figure 2.6: In the left picture one silicon-detector with the front-end electronic boards and kapton plat cables is shown; in the right picture the final assembly for one detector including the cooling plate for the electronic board is displayed. Figures taken from [42].

- the setup has to be arranged in an azimuthal symmetry (left-right) in ϕ to use the double-ratio method for the asymmetry measurements, that serve to calculate the beam polarization and analysing powers, see Chapter 3.

- events with proton and deuteron tracks should be in the detector

acceptance to allow for the setup alignment.

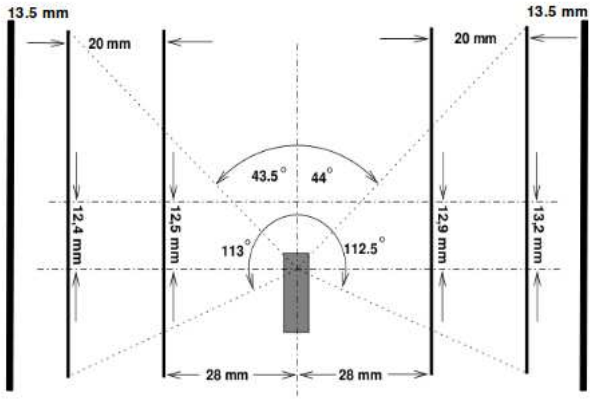

Figure 2.7: Schematic view of the zx plane of the detector (the beam is along the z direction). Target position and distances bewteen layers are indicated.

The beam polarization P is determined using the left-right asymmetry ϵ of the scattered deuterons. This asymmetry is proportional to the analysing power A_y of the *pd* elastic scattering through the relation:

$$\epsilon = P \cdot A_y. \tag{2.1}$$

The STT is placed in the region where the *pd* elastic Figure Of Merit (FOM) defined by:

$$FoM = \frac{d\sigma}{d\Omega(\theta_{cm})} \cdot (A_y(\theta))^2, \tag{2.2}$$

exhibits the maximum value.

According to experimental data at $T_p = 46.3$ MeV, see Fig.2.8, it is taken in consideration the FOM value at θ^p_{cm}=110^o (that in the laboratory is $\theta^p_{lab} = 80^o$), since the first peak corresponds to angles in the forward scattering region where it is not possible to place the STT.
To optimize the FOM the STT was placed 12 mm downstream along the beam direction. The first layer is placed at 28 mm from the center of the beam pipe to protect the detector; the distance between first and second layer is 20 mm. The distance between second and third layer is 13.5 mm. The trigger signal was produced when at least one track was generated in the detection system and this corresponds to a coincidence between both sides of every second layer.

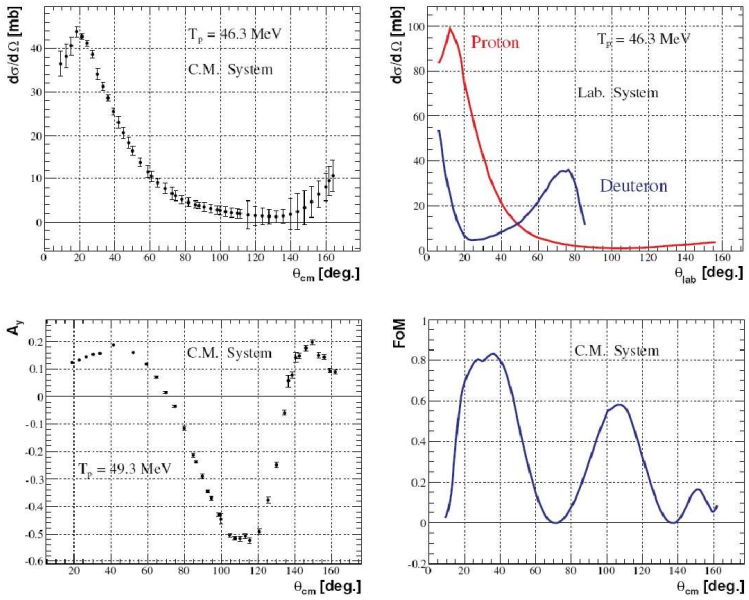

Figure 2.8: In the upper panels the *pd* elastic differential croos section is represented in the center of mass and laboratory system. In the lower panels the Analysing power A_y and the Figure of Merit FoM of the *pd* elastic scattering in the center of mass system are displayed.

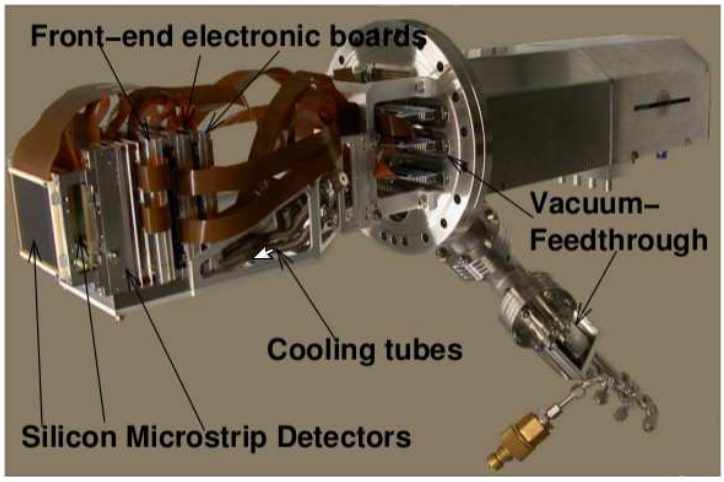

Figure 2.9: The complete setup of a Silicon Tracking Telescope is shown. The three silicon microstrips sensors are indicated as well as the kapton flat cables that link the detector to the the front-end electronic boards, and the vacuum feedthrough.

Chapter 3

Deuteron Breakup events analysis

The pd $\rightarrow$ ppn Deuteron Breakup channel has been studied using Monte Carlo and experimental data.
The ultimate goal of the analysis is the selection of *pd* Breakup and in particular the identification of the neutron. The identified *pd* Breakup events are used to develop a method for calculating the analysing powers A_y of *pd* Breakup with respect to the neutron.
The presented data had been taken during the February 2008 beam time, when an experiment to test the possibility of using unpolarized electrons to depolarize an initially polarized proton beam was performed at the COSY-ring. A polarized proton beam was stored in COSY and the electrons of the electron-cooler have been employed as free electron target. The depolarization of the beam ,caused by the interactions with the electrons, was monitored measuring the beam polarization by means of the proton-deuteron elastic scattering events induced at the deuteron cluster target [32].
In these experimental conditions, proton-deuteron collisions can give rise to Deuteron Breakup events. Since the experimental setup is able to identify this reaction, Deuteron Breakup channel can be studied as a complete independent Physics case.
In this chapter the data analysis procedure to reconstruct Deuteron Breakup events, in simulated and experimental data, and in particular the selection criteria developed to tag this reaction are described. The identified deuteron breakup events are employed in the method development for the measurement of the analysing power A_y of *pd* Breakup

with respect to the neutron.

3.1 *pd* Breakup vs *pd* elastic

When a proton beam of 49.3 MeV kinetic energy impinges on a deuterium target, two channels can be accessible: *pd* elastic scattering $pd \rightarrow pd$ and Deuteron Breakup $pd \rightarrow ppn$. In the experimental data these two channels are present together and need to be separated.

While the phase space of the *pd* elastic channel is well defined, the *pd*

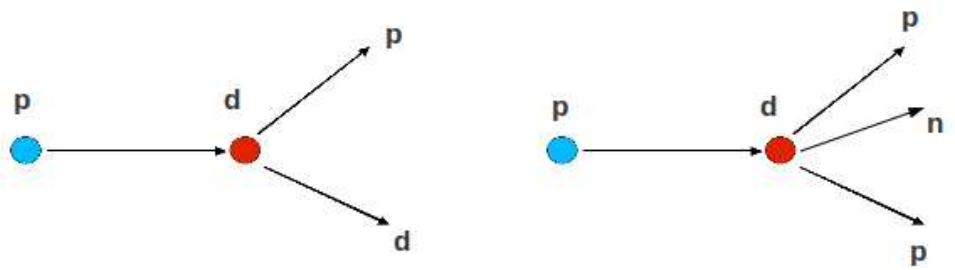

Breakup, being a three-body final state reaction, occupies a broader phase space which overlaps to the elastic one. The basic idea to isolate the *pd* Breakup channel is to exclude the *pd* elastic channel from the phase-space and get all the infomations from the two outgoing protons. This second requirement is necessary since the neutron is invisible for the used detection system and *pd* Breakup could be identified when the two outgoing protons stop inside the detector acceptance. Once the two protons are stopped, using the four momentum conservation, the complete kinematic can be determined. The four-momentum of the missing neutron is given by:

$$n^{\mu} = p^{\mu}_{Beam} + d^{\mu}_{Target} - p^{\mu}_{1,Telescope} - p^{\mu}_{2,Telescope}, \tag{3.1}$$

in which p^{μ}_{Beam} is the four-momentum of the incoming proton, d^{μ}_{Target} the four-momentum of the deuteron target (it is a fixed target, so it coincides with the deuteron mass), $p^{\mu}_{1,Telescope}$ and $p^{\mu}_{2,Telescope}$ the four-momentum of two outgoing protons detected and stopped in the telescopes.

In order to maximize the number of stopped protons, a third thicker silicon layer was installed to increase the stopping power.

Once the protons from *pd* Breakup events are selected, the Missing Mass:

$$M_{missing} = \sqrt{(E^{p}_{Beam} + m_d - E_{p1} - E_{p2})^2 - (\overrightarrow{p}^{p}_{Beam} - \overrightarrow{p}_{p1} - \overrightarrow{p}_{p2})^2} \tag{3.2}$$

is used as a control criteria to tag the reaction and it should peak at the Neutron mass 939.57 MeV/c^2. In equation 3.2, E^{p}_{Beam} and $\overrightarrow{p}^{p}_{Beam}$ are the total energy and 3-momenta of the incoming proton, m^d the deuteron mass, 1875.61 MeV/c^2, E_{p1},E_{p2} are the total energies of the two outgoing protons, $\overrightarrow{p}_{p1}$ and $\overrightarrow{p}_{p2}$ are the 3-momenta of the two outgoing protons.

3.1.1 Kinematics of $pd \rightarrow ppn$

In general in a reaction $A + B \rightarrow 1 + 2 + 3$ with two initial particles and three particles in the final state, $3 \times (2 + 3)$ momenta components have to be defined. The momentum-energy conservation laws fix four relations between momenta components of the particles in the initial and final state; moreover if the center of mass system is used, one can define three conditions for the initial state derived by:

$$\overrightarrow{p}^{c.m.}_{A} + \overrightarrow{p}^{c.m.}_{B} = 0, \tag{3.3}$$

and three conditions for the final state:

$$\overrightarrow{p}^{c.m.}_{1} + \overrightarrow{p}^{c.m.}_{2} + \overrightarrow{p}^{c.m.}_{3} = 0. \tag{3.4}$$

Therefore a three-final state channel can be described by means of $3 \times (2 + 3) - 4 - 3 - 3 = 5$ independent variables.

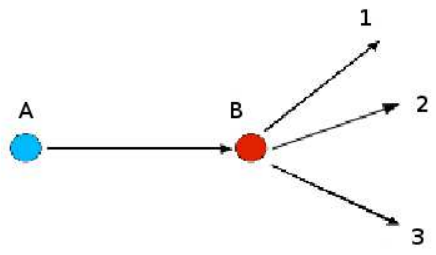

In the case of *pd* Breakup reaction the five independent variables can be: θ_p,θ_q,ϕ_p and ϕ_q, which are the polar and azimuthal angles of

the jacobi momenta p and q, and the excitation energy of the proton pair E_{pp} defined as:

$$E_{pp} = \sqrt{(E_{p1} + E_{p2})^2 - (\overrightarrow{p}_{p1} + \overrightarrow{p}_{p2})^2} - 2m_p, \tag{3.5}$$

where E_{p1},E_{p2},$\overrightarrow{p}_{p1}$ and $\overrightarrow{p}_{p2}$ are the total energies and the 3-momenta of the two outgoing protons and m_p is the proton mass.

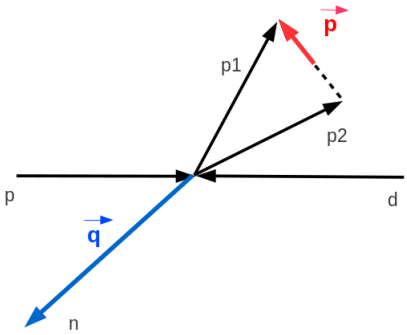

Figure 3.1: Jacobi momenta of $pd \rightarrow ppn$ in the center-of-mass system. p=1/2(p1+p2) and q=-(p1+p2).

3.2 Simulations and Data

The data analysis is divided in two stages: one concerning Monte Carlo simulations and the other experimental data.
In order to estimate the expected detector performances and in particular to study the reconstruction efficiency for *pd* Breakup events and the *pd* elastic contamination, different samples of simulated *pd* Breakup and *pd* elastic events have been analyzed, implementing the February 2008 detector configuration.
The *pd* elastic scattering is generated based experimental data[33]. The low energy *pd* Breakup is generated in the framework of the pure phase-space GENBOD model with the proton beam kinetic energy of 49.3 MeV. The GEANT package [34] was used for the detector response. The output of the simulations consists of a list of events containing hits informations like spatial coordinates, angles and deposited energies.
The Monte Carlo data study allowed the tuning of the selection criteria that serve to optimize the *pd* Breakup identification efficiency.

Simulated channel	Number of generated events
pd→ pd	10^6, T_p =49 MeV
pd→ ppn	10^6, T_p=49 MeV

Table 3.1: This table displays Monte Carlo informations concerning the channel simulated and the number of generated events for each channel.

Concerning experimental data, the execution of the primary data analysis, energy calibration correction, hits and tracking analysis is controlled by the *Rootsorter* framework software developed at IKP[35]. The output is arranged in a list of events with complete event identification data (i.e. time, beam polarization index, target polarization, etc.) and hits informations. Each hit contains the information about the energy loss of the particle and its position in the detector. In the next section the track reconstruction and the *pd* Breakup identification techniques (used either in Monte Carlo or data) are described.

3.2.1 RUN SELECTION

The data taking was performed with 10^8 stored protons. For this analysis seven runs have been analyzed. During each run the proton beam polarization was alternated between state UP (↑), DOWN (↓) and unpolarized (0). The geometry is represented in Fig.3.2. During the beam time the third layer in one telescope was not working.

Date	RUN	Start	Stop	Events
Feb 03,2008	260	16:49	17:00	1360305
Feb 03,2008	262	17:06	17:16	1364067
Feb 03,2008	264	17:16	17:26	1362196
Feb 03,2008	266	17:26	17:36	1350207
Feb 03,2008	267	17:36	17:58	1368407
Feb 03,2008	270	18:15	18:27	1352119
Feb 03,2008	272	18:36	18:50	1174226

Table 3.2: This table contains some informations on the runs of February 2008 analysed for this thesis. The start and stop time and the number of stored events are indicated.

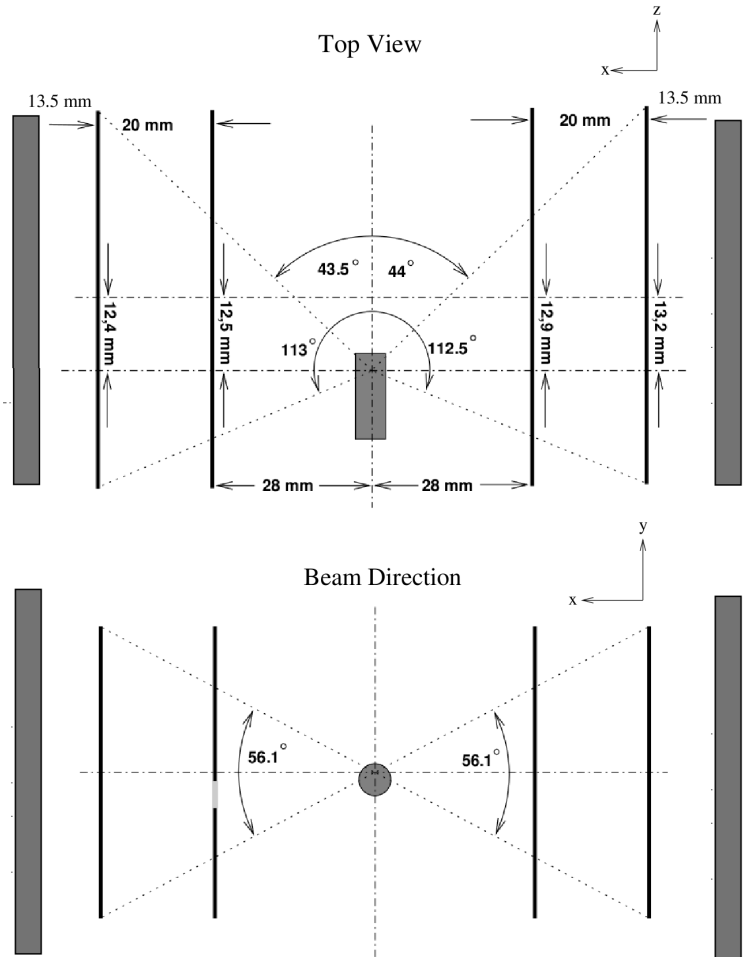

Figure 3.2: In the upper figure, the zx plane of the detector is shown. The proton beam is directed along the positive side of the z axis. The proton beam polarization is directed along y-axis. The indicated angles show the geometrical acceptance of the polar angle when a scattered particle impinges on the first two layers. In the lower figure, the yx plane, looking in the beam direction, is shown.

3.3 Track Reconstruction

A track is defined as a straight line between two correlated hits in the first two layers. Firstly contiguous signals (within a radius of 1 mm) in the silicon strips are merged together into the so-called silicon hits. Only events with at least two hits in the first layers and one hit in the second layer of the detector are considered. Secondly the candidate tracks are reconstructed from one hit in the first and one hit in the second silicon layer if they are separated by less than 6 degrees

in azimuthal angle.
A hit in the third silicon layer is linked to the reconstructed track if its distance from the extrapolated point of the track is less than 1 cm.
In events where two tracks are traced, the method of distance of closest approach is applied to reconstruct the interaction vertex. Whereas in events in which only one track is traced, the method of distance of closest approach is applied between the track and the beam line to localize the vertex point; after that the second track is traced connecting the vertex point to the coordinates of any untraced hit in the first layer.
Three track typologies are considered: track "1", if the particle stops into the first layer, track "2" and "3", if the particle stops into the second or the third layer respectively, see Fig.3.3.

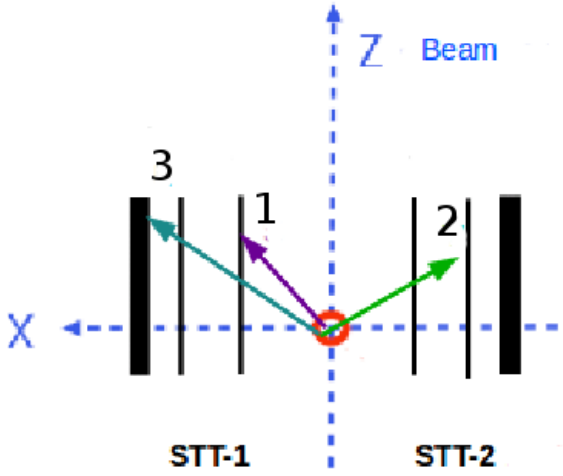

Figure 3.3: Schematic view of the zx detector plane in which track 1,2 and 3 are represented.

In Monte Carlo, *pd* elastic and *pd* Breakup channels can be switched on separately, whereas in data they are present together; the first part of the analysis is dedicated to the identification and separation of the two reactions.
The request to suppress the elastic channel to negligible contribution is realized applying a co-planarity cut, shown in Fig.3.4. This cut, in addition to the request of having no deuterons in the final state, provides the elastic and breakup channel separation.

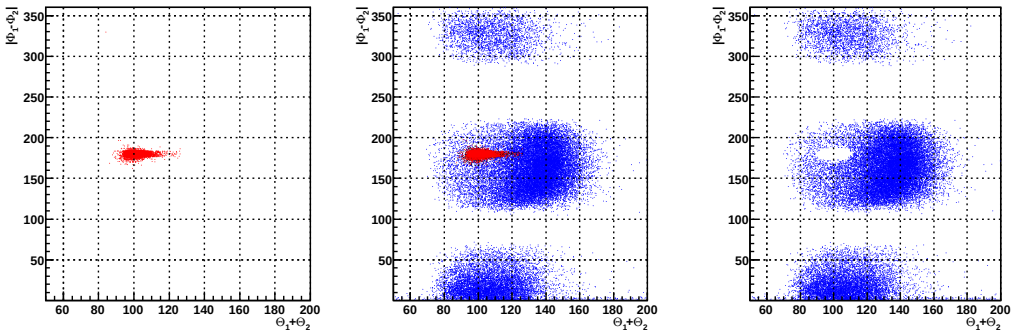

Figure 3.4: Monte Carlo: the co-planarity cut. The relation between the polar angles of the 2-outgoing particles versus their azimuthal angle is displayed. The left panel shows the phase space of the pd elastic channel in simulations, the middle panel shows the phase space of the pd elastic (red) and pd Breakup channel (blue) together, the right panel displays the phase space of pd Breakup in which the ellypse-like area of pd elastic has been excluded; in this way the main concentration of pd Breakup remains.

3.3.1 Particle Identification

The energy loss information carried by hits provides the selection of the charged particles by the ΔE/E and Particle IDentification (PID) methods. These two methods are developed combining the energy loss detected in the Silicon Tracking Telescope and the energy loss of particles in matter, as described by the Bethe-Block formula:

$$-\frac{dE}{dx} = \frac{4\pi n z^2}{m_e v^2} \cdot (\frac{e^2}{4\pi\epsilon_0})^2 \cdot ln\frac{2m_e v^2}{I}, \tag{3.6}$$

where v is the velocity of the incoming particle, ϵ_0 the vacuum permittivity, m_e the electron mass, n the electron density, z the atomic number and I the average ionization energy.
Showing E_1, the deposited energy in the first layer, as function of E_2 the deposited energy in the second layer, one can see that different particles populate different regions of the phase-space ($\Delta E/E$ method). The borderline of these regions is broad since the particles pass through more or less detector material depending on the incident angles.

To simplify proton/deuteron separation, the PID method can be applied; in this case the energy loss are parametrized by the so-called c parameter defined as follow:

$$c = (E_1 + E_2)^{1.62} - E_2^{1.62}. \tag{3.7}$$

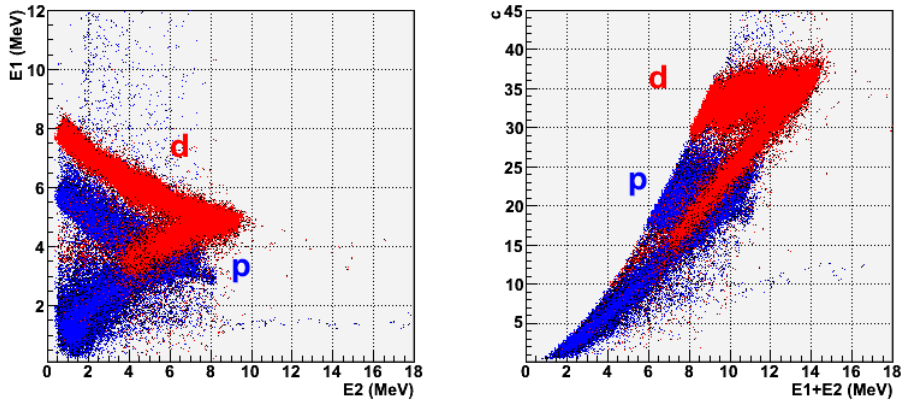

Figure 3.5: Monte Carlo pd elastic and pd Breakup together. In the left panel the ΔE/E plot is shown. In Monte Carlo a flag tags particles as protons (blue points) or deuterons (red points); protons and deuterons populate different loci of the phase space. Looking at the deuterons (same is for protons), the upper band corresponds to particles stopped in the 2^{nd} layer acceptance and the lower band corresponds to deuterons having enough energy to pass through the 2^{nd} layer. Here deuterons can miss the 3^{rd} layer or can enter the 3^{rd} layer and stop because of its thickness. In this region deuterons lay on the stopped protons band. If these deuterons enter the 3^{rd} layer, they can be separated from protons, otherwise the separation between protons and deuterons is not applicable. In the rigth panel the PID cut is shown. Using an energy parametrization it is possible to convert the left plot in the right one in which the protons-deuterons separation is realized applying a horizontal cut.

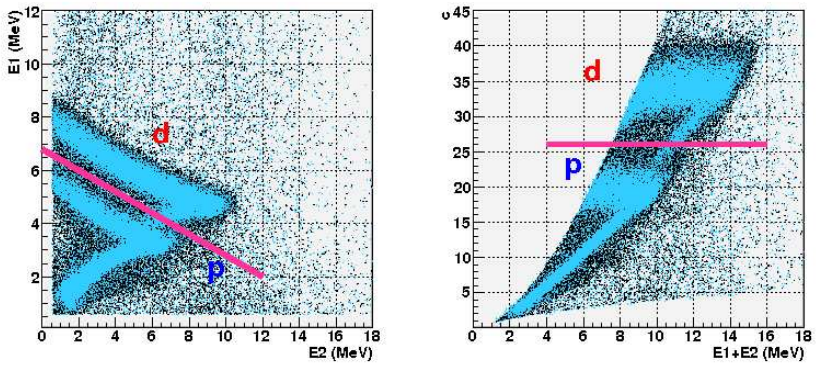

Figure 3.6: Experimental data. In the left panel the ΔE/E plot is shown, a flag indicating protons or deuterons is no longer available. The selection of protons and deuterons can be carried out with a linear cut (magenta line) which divides the plane in protons and deuterons loci. The same considerations for the overlapping protons-deuterons regions are applied here. In the rigth panel the PID cut is shown, the separation is realized using a horizontal cut (magenta line).

A cut around the horizontal band (see Fig.3.6) allows the separation between protons and deuterons.
After having separated the two channels, the further step of the analysis is aimed to identify the tracks with two protons stopped in the detector.

3.3.2 Track "1" reconstruction

When a particle stops in the first layer is labelled as track "1". Track "1" is selected by means of a geometrical cut in which the particle is supposed to have one hit in the first layer and its track, originating from the target region, is projected in the forward direction to check if it intercepts the second layer acceptance. Since the particle identification is not applicable in the first layer, to eliminate the high background from deuterons stopped in the first layer, a co-planarity cut is required.

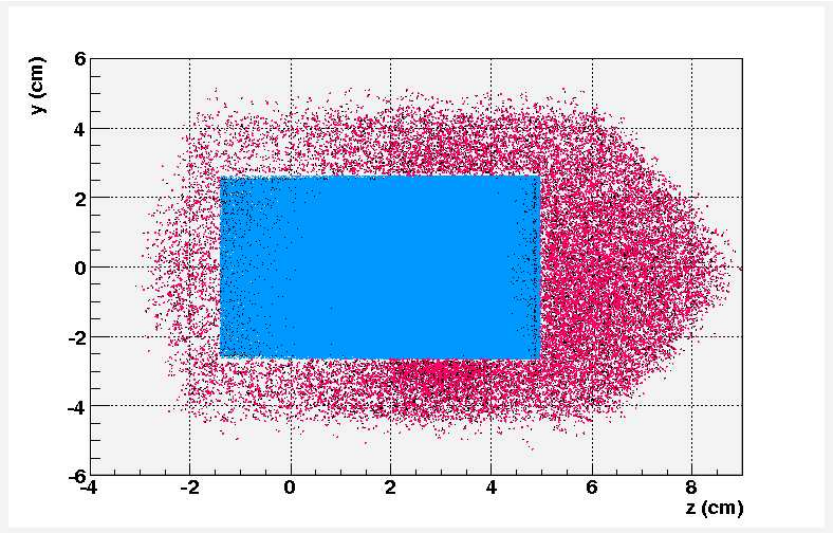

Figure 3.7: Selection of proton track "1". YZ plane of the second layer. The cyan points refers to the nominal position of the 2^{nd} layer; the pink points are projections of tracks with one hit in the 1^{rst} layer that miss the 2^{nd} layer acceptance. If a projection belongs to the 2^{nd} layer acceptance and no correlated hit is found then it is labelled as track "1".

3.3.3 Track "2" reconstruction

Track "2" refers to particles stopped in the second layer of the detector. Stopped particles are selected using ΔE/E and Particle IDen-

tification (PID) methods. Particles displayed in Fig.3.6 are those that pass the first layer and give rise to a signal in the second layer. Particles with the highest energy loss in the first layer have a low energy loss in the second; as the energy of the particle increases, the energy loss in the second layer increases and the deposited energy in the first layer decreases, since the energy loss is proportional to $1/v^2$. The upper

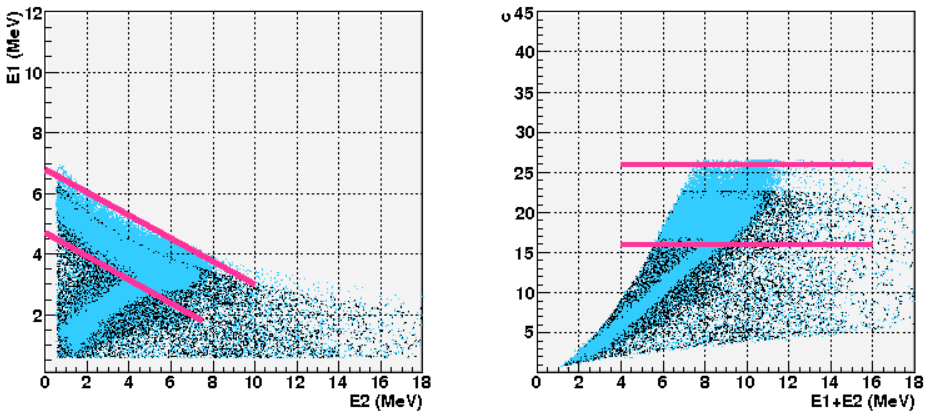

Figure 3.8: Experimental data. In the left panel the ΔE/E plot and in the right panel the PID plot are displayed in both cases without the deuterons loci; here the main concentration of pd Breakup has been identified. Protons stopped in the second layer are isolated selecting the band bounded by the pink lines.

bands are populated by deuterons and protons respectively stopped in the second layer and their initial kinetic energy is determined by the sum of the deposited energy in the first two layers. The lower bands are populated by protons and deuterons that pass through the second layer acceptance and can enter the third layer. Restricting our analysis to protons, the selection of a track "2" proton is carried out with these requirements: first two layers fired, the particle should lay on the stopped protons regions (see Fig.3.8) and no hits on the third layer.

3.3.4 Third layer Calibration

Before discussing the reconstruction of Track "3", it is here presented the calibration procedure of the third layer. The thickness of the third layer required the use of capacitors to accomplish the attenuation of the input signal, therefore the deposited energies have to be calibrated to get the correct value. At this aim, the ΔE/E plots (2^{nd}

versus 3^{rd} layer) in Monte Carlo and experimental data have been compared in order to make them coincide.
The results of this calibration has the effect of shifting the peak of the Missing Mass distribution to the correct value, as reported in Fig.3.11.

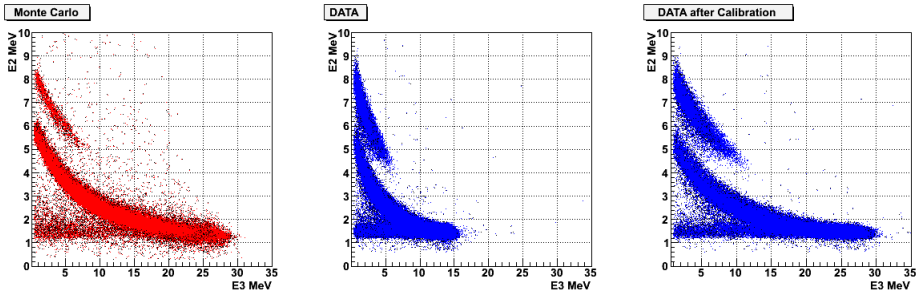

Figure 3.9: The ΔE/E plot displaying the energy loss in 2^{nd} layer versus energy loss in 3^{rd} layer is shown for Monte Carlo (left panel) and experimental data (right panels). The middle panel shows experimental data without the calibration, the right panel represents experimental data after the energy calibration. The calibration has been realized making the energy losses shown in the first and second panel coincide.

3.3.5 Track "3" reconstruction

A track labelled as "3" is originated by a particle stopped in the third layer and is selected using the plot representing E_2, the energy loss in the second layer, as a function of E_3, the energy loss in the third layer. The upper band refers to deuterons entering the third layer. Deuterons that reach the third layer, due to its thickness, are here stopped. The lower band in the ΔE/E plot refers to protons. Also in this case a parametrization of the deposited energies can be used to disantangle protons and deuterons and to identify the stopped particles:

$$c_3 = (E_1 + E_2 + E_3)^{1.7} - E_3^{1.7} \tag{3.8}$$

The selection of a "3" track proton is made looking for 3-hits tracks in the proper region of the phase space of protons stopped in the third layer, as indicated in Fig.3.10.

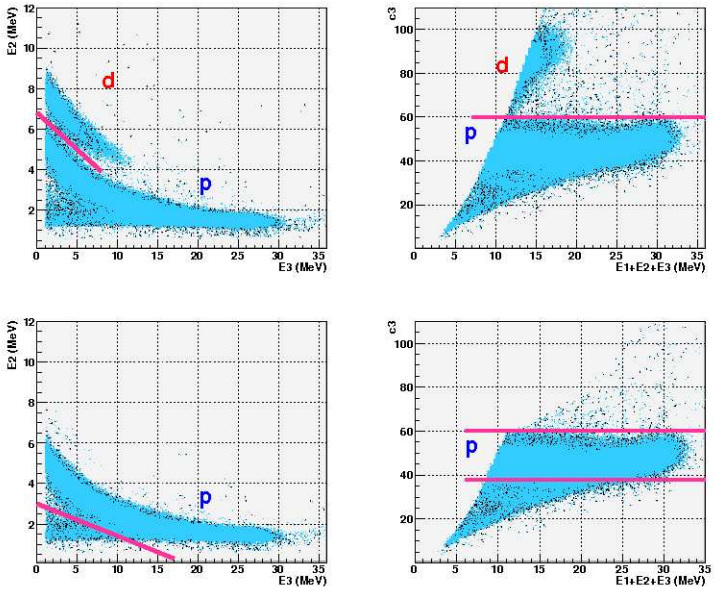

Figure 3.10: Experimental data. In the upper box the ΔE/E plot (left panel) for 2^{nd} and 3^{rd} layer and its parametrization PID plot (right panel) are shown, considering pd elastic and pd Breakup. Applying the cut identified by the pink line, one can select protons or deuterons. In the lower panel ΔE/E plot and PID plot without pd elastic. Protons labelled as track "3" are isolated applying the cut indicated by the pink lines, which selects the protons stopped in the 3^{rd} layer.

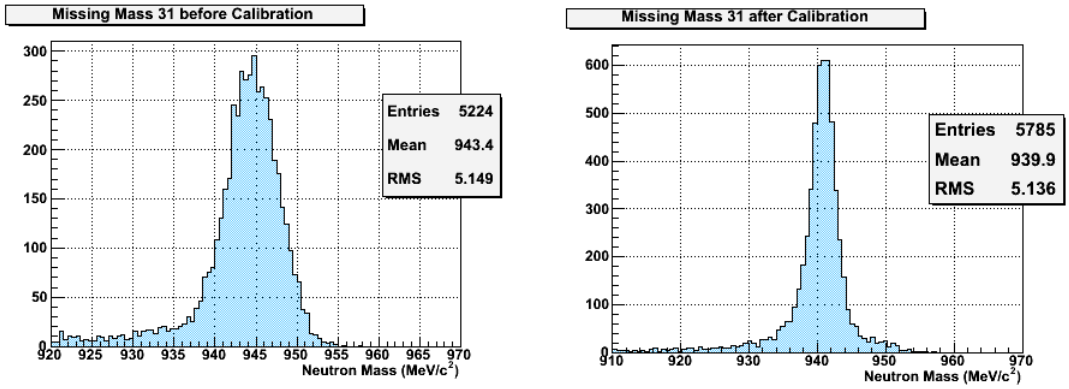

Figure 3.11: Experimental data: run 260. The Missing Mass distribution is shown before and after the calibration of the third layer.

3.4 Deuteron Breakup samples

The combination of two stopped-protons tracks (1,2 or 3) generates five event samples labelled 2-1, 2-2, 3-1, 3-2, 3-3 referring to the number of hits in each track. These event samples are investigated separately as they populate different loci of the phase space. Every sample is identified by means of a combination of the selection criteria described above.

- 2-1 sample: This category is identified applying the c parameter cut and the track "1" geometrical cut. In addiction the co-planarity cut is applied because of the high background of deuterons stopped in the 1^{rst} layer.

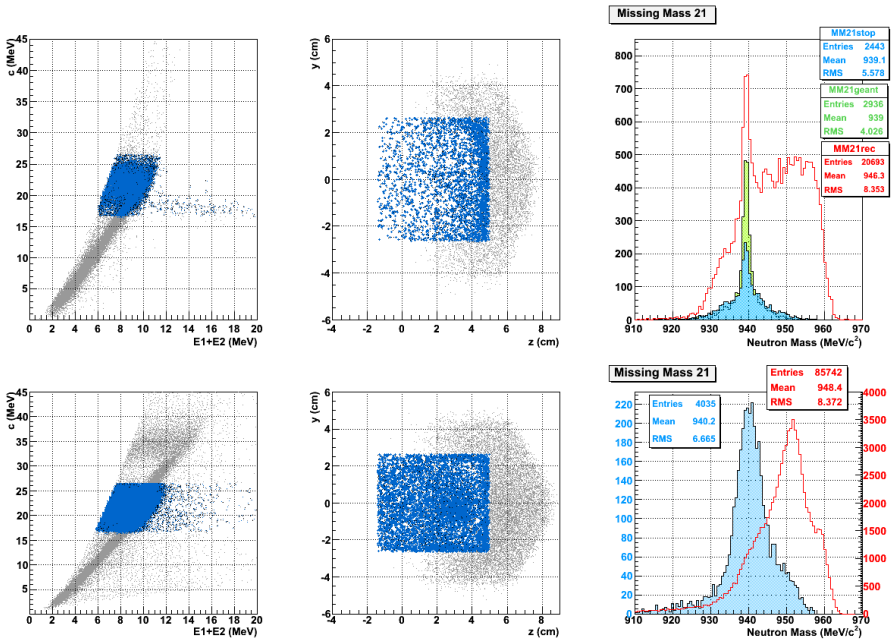

Figure 3.12: 2-1 sample. Upper panels: Monte Carlo. The left panel shows the selection to identify the protons stopped in the 2^{nd} layer, the middle panel shows the geometrical cut on the projection of the track to identify protons stopped in the 1^{rst} layer. The right panel displays the Missing Mass distributions: the red one refers to reconstructed events (21s events that enter the geometrical acceptance but not necessarily stopped), the green one refers to generated stopped events (21s events that are stopped according to simulations), the blue one refers to the events stopped using the selection criteria. Lower panels: DATA. Starting from the left the selections to identify stopped protons in the 2^{nd} and 1^{rst} layer are shown. In the right panel the Missing Mass for reconstructed (red) and stopped (blue) 21s events.

- 2-2 sample: This category is identified applying the c parameter and the co-planarity cut.

- 3-1 sample: This sample is identified applying the c3 parameter (eq.3.8) and the track "1" geometrical cut; the co-planarity cut is applied for the reason already mentioned for the 2-1 sample.

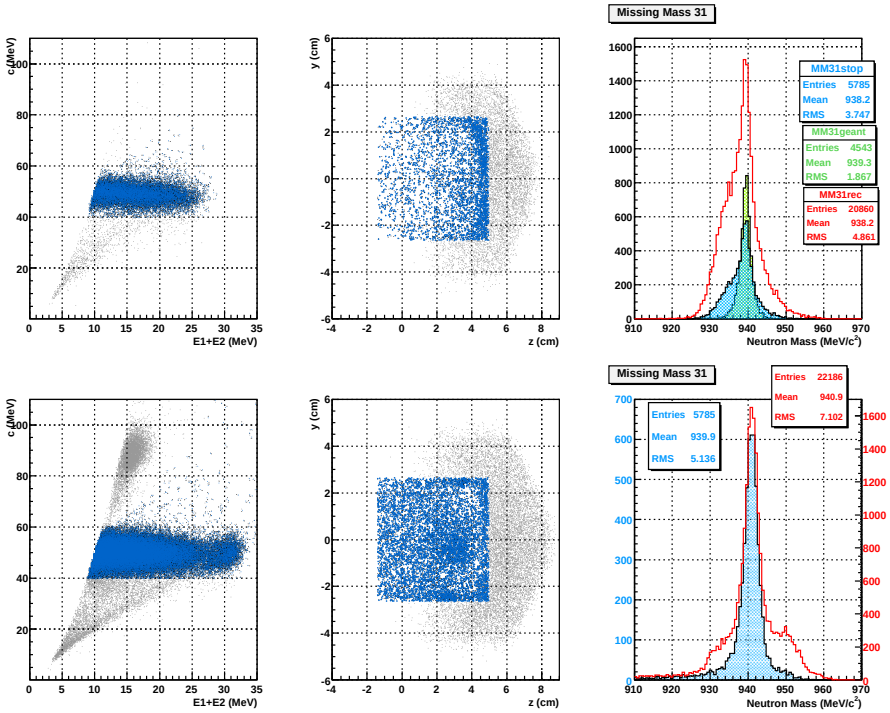

Figure 3.13: 3-1 sample: in the upper panels: Monte Carlo. The left panel shows the selection to identify the protons stopped in the 3^{rd} layer. In the middle panel, the cut for protons stopped in the first layer is represented. The right panel displays the Missing Mass distributions: the red one refers to reconstructed events, the green one refers to generated stopped events, the blue one refers to the events stopped using the selection criteria. Lower panels: DATA. Same plots as mentioned above but displayed for data. In the right panel the Missing Mass for reconstructed (red) and stopped (blue) 31s events.

- 3-2 sample: This sample is identified applying the c3 parameter (eq.3.8) and the c parameter (eq.3.7) selection; the request of the coincidence of two stopped protons makes the co-planarity cut not necessary in this sample.

3.5 Efficiency of Breakup identification

The Missing Mass of the different samples are shown for Monte Carlo, see Fig.3.14 and data, see Fig.3.15. The Missing Mass is applied as a control criteria to tag a breakup event. The number of events identified for each run is displayed in Table 3.2.

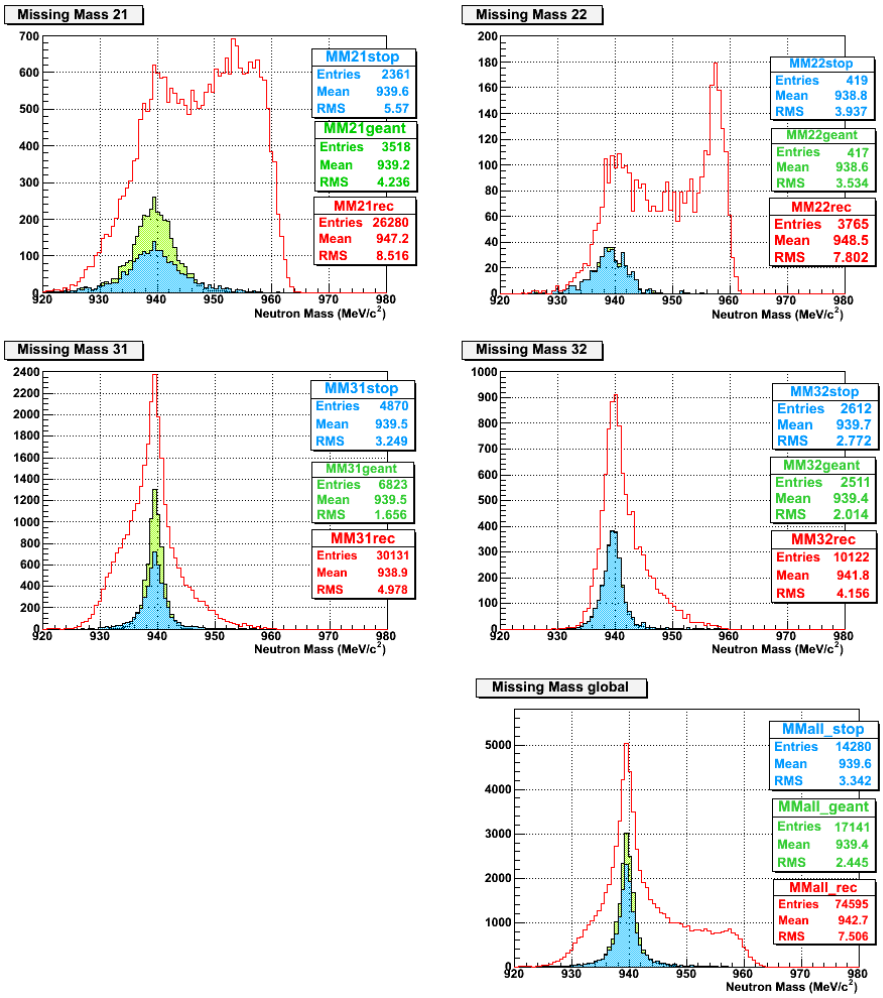

Figure 3.14: Monte Carlo. The Missing Mass distribution is shown for the Breakup event samples invidually and together (bottom right). RED: the Missing Mass for reconstructed events (events not necessary stopped inside the detector acceptance), GREEN: the Missing Mass for generated stopped events (events in which generated and reconctruted energy coincides), BLUE: the Missing Mass for stopped events (events identified with selection criteria).

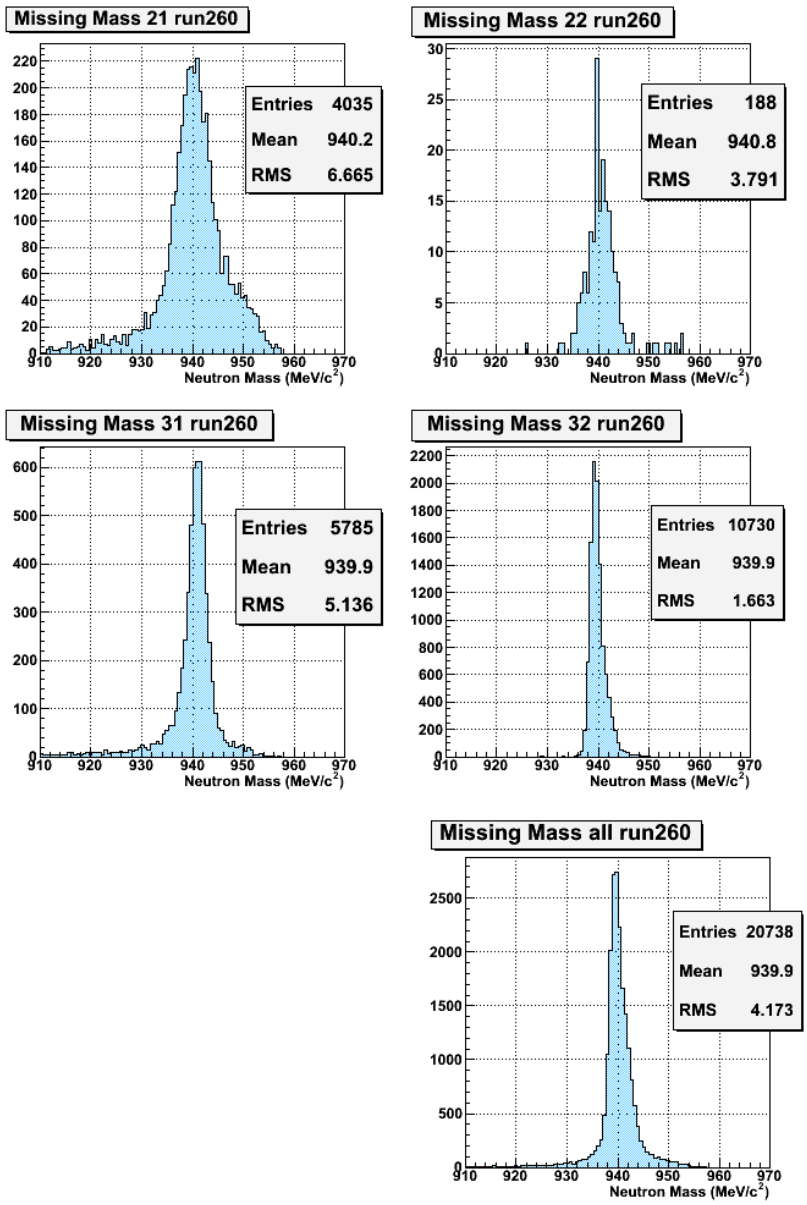

Figure 3.15: Experimental data: The Missing Mass distribution is shown for the Breakup event samples invidually and together (bottom right) for a single run. These distributions refer to stopped events (events identified with selection criteria).

MONTE CARLO					
Monte Carlo	**21**	**22**	**31**	**32**	**ALL**
Reconstructed	26280	3765	30131	10122	74595
Truly Geant Stopped	3518	417	6823	2511	17141
Stopped	2361	419	4870	2612	14280

Table 3.3: Monte Carlo statistics: this table contains the number of reconstructed events (events that enter the detector acceptance but nit necessarily stopped), truly geant stopped events (events in which generated and reconstructed energies coincide) and stopped events (events that fulfill the selection criteria). The counts are reported for each sample and all together.

DATA					
RUN	**21**	**22**	**31**	**32**	**ALL**
260	4299	188	5785	10730	21002
262	4073	162	5843	10780	20858
264	4178	145	5795	10741	20859
266	4015	189	5771	10409	20384
267	3821	174	5701	10305	20001
270	3489	165	4948	9265	17867
272	3178	131	4841	9055	17205

Table 3.4: Number of identified deuteron breakup events for each sample and for all samples considered together in experimental data. The presence of the third layer of 5mm increases the stopping effiency by a factor 3 with respect to the stopping efficiency of the first two layers. The 3-3 sample is not considered since one of the third layer was not working during the whole beam time.

3.6 Phase Space Coverage

The identified Breakup samples populate different regions of the phase space. The jacobi momenta of the identified samples are displayed in Fig.3.16, 3.17, 3.18, 3.20, 3.21, 3.22, 3.23 to show the phase space coverage.

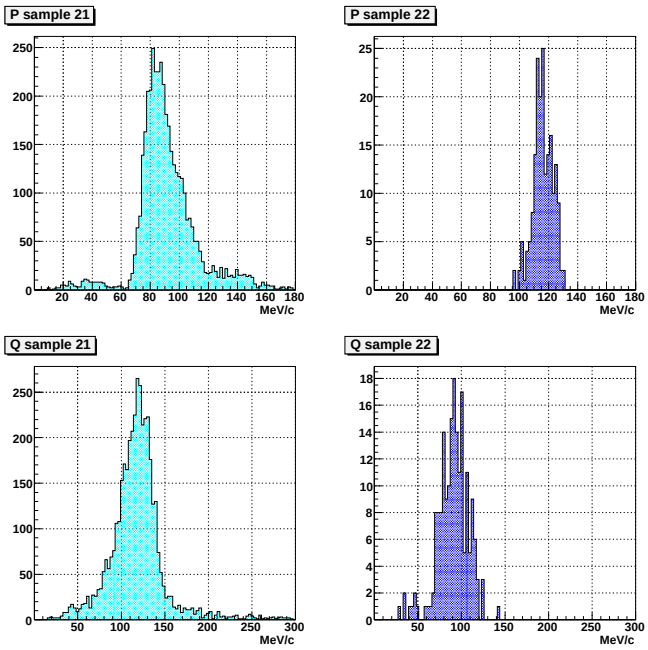

Figure 3.16: Experimental data: Jacobi momenta **p** and **q** for 2-1 and 2-2 samples. In particular, **q** represents the neutron in the center of mass system.

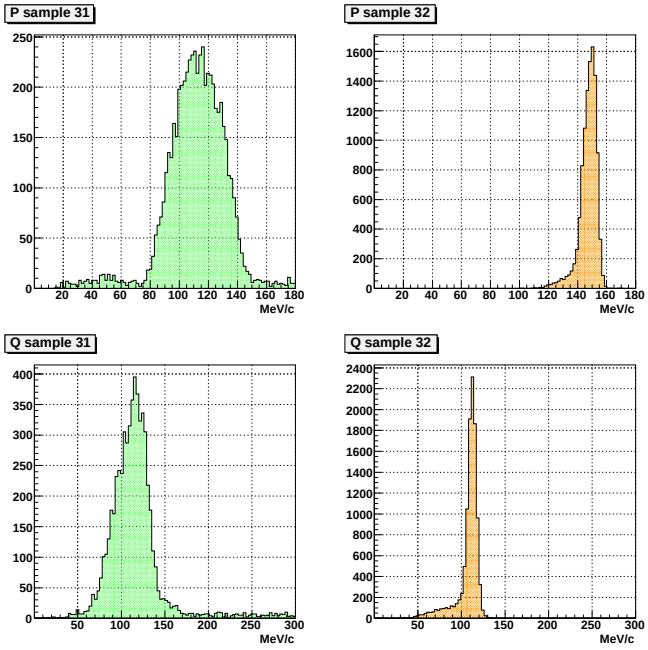

Figure 3.17: Experimental data: Jacobi momenta **p** and **q** for 3-1 and 3-2 samples. In particular, **q** represents the neutron in the center of mass system.

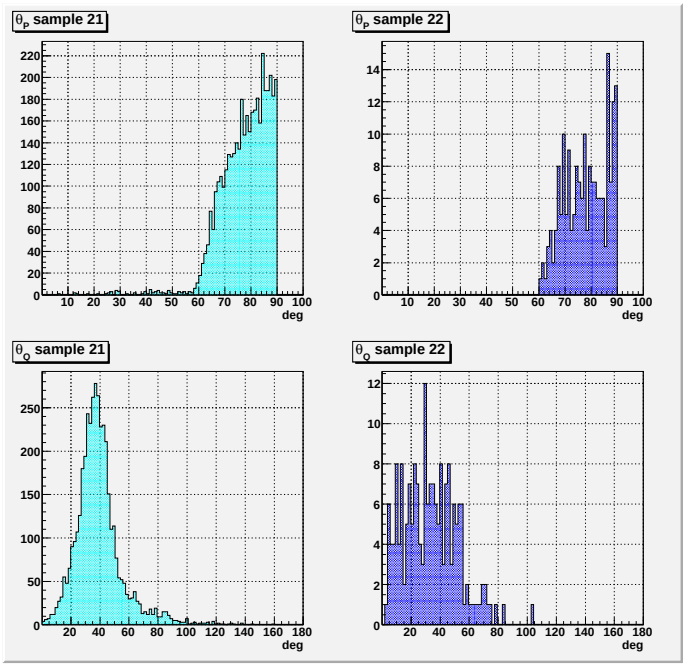

Figure 3.18: Experimental data: Polar and azimuthal angles of **p** and **q** for 2-1 and 2-2 samples.

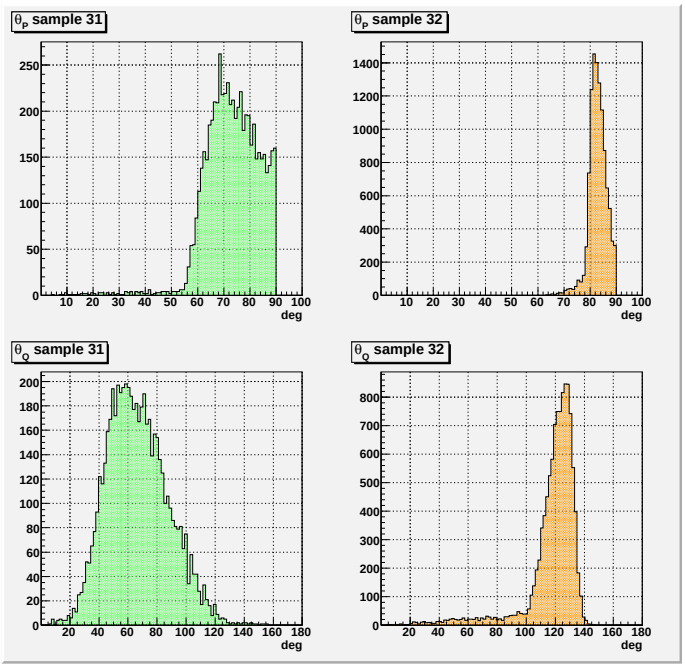

Figure 3.19: Experimental data: Polar and azimuthal angles of **p** and **q** for 3-1 and 3-2 samples.

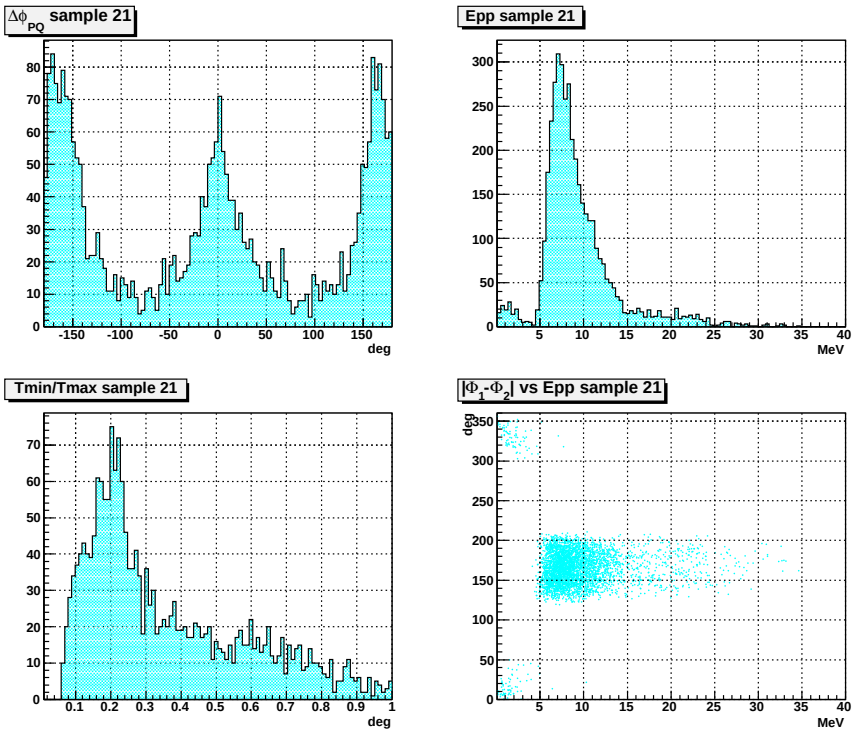

Figure 3.20: Experimental data: 2-1 sample. $\Delta\phi_{pq}$ and the excitation energy E_{pp} are shown in the upper panels. In the lower left panel the ratio between the kinetic energies of the two outgoing protons is shown, Tmin (max) refers to the kinetic energy of the less (more) energetic proton. In the lower right panel it is shown the relation between the relative outgoing direction of the two protons and the excitation energy. In this sample there are events in which both protons are impinging on the same telescope and populate the phase space region in which the absolute value of the difference of the two azimuthal angles is close to 0 and 360 degrees. The concentration of events around 180^o refers to protons directed towards different telescopes.

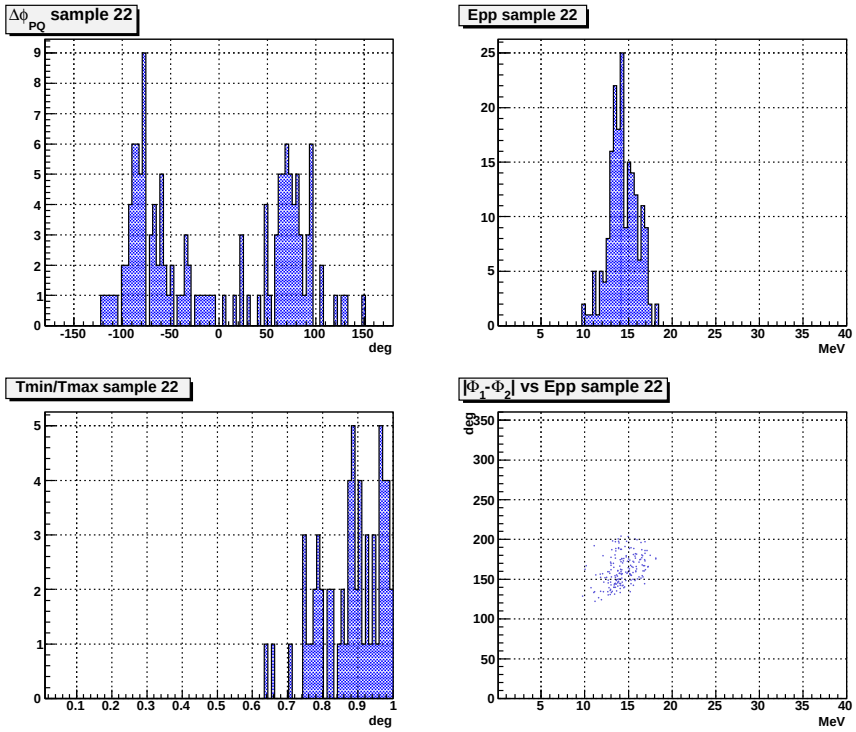

Figure 3.21: Experimental data: 2-2 sample. $\Delta\phi_{pq}$ and the excitation energy E_{pp} are shown in the upper panels. In the lower left panel the ratio between the kinetic energies of the two outgoing protons is shown. In the lower right panel it is shown the relation between the relative outgoing direction of the two protons and the excitation energy. In this sample the two outgoing protons have the same energy and are emitted simmetrically with respect to the interaction point. For this reason they populate the region around 180^o.

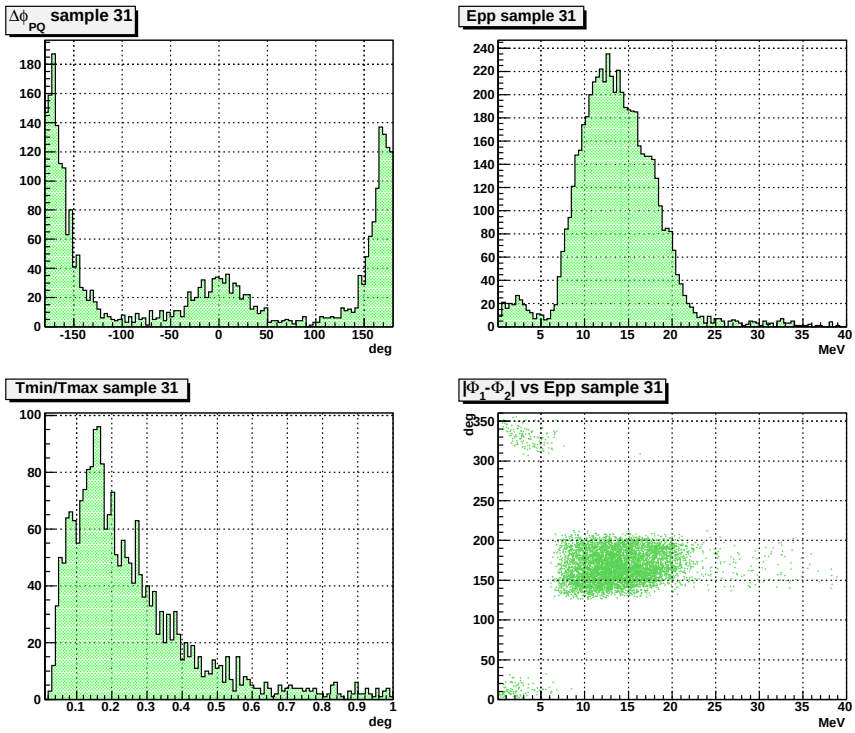

Figure 3.22: Experimental data: 3-1 sample. $\Delta\phi_{pq}$ and the excitation energy E_{pp} are shown in the upper panels. In the lower left panel the ratio between the kinetic energies of the two outgoing protons is shown. In the lower right panel it is shown the relation between the relative outgoing direction of the two protons and the excitation energy. In this sample there are events in which both protons are impinging on the same telescope and populate the phase space region in which the absolute value of the difference of the two azimuthal angles is close to 0 and 360 degrees. The concentration of events around 180^o refers to protons directed towards different telescopes.

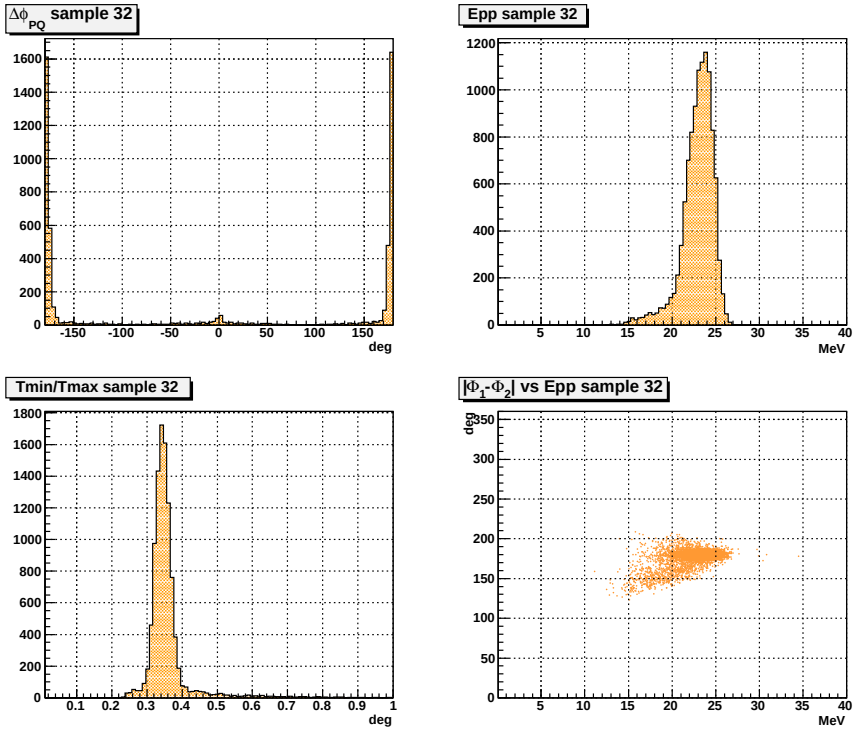

Figure 3.23: Experimental data: 3-2 sample. $\Delta\phi_{pq}$ and the excitation energy E_{pp} are shown in the upper panels. In the lower left panel the ratio between the kinetic energies of the two outgoing protons is shown, Tmin (max) refers to the kinetic energy of the less (more) energetic proton. As in the 2-2 sample case, the two outgoing protons are emitted towards different telescopes.

3.7 Method development for the analysing power A_y in pd→ppn

In this section the algorithm to calculate the analysing power in *pd* breakup with respect to the neutron is presented.
The notation to define the analysing power is reported here. The spin dependent differential cross section for a spin 1/2 beam impinging on an unpolarized target is:

$$\frac{d\sigma}{d\Omega}(\Theta,\phi) = \frac{d\sigma_0}{d\Omega}(\Theta)\cdot[1 + P\cdot A_y\cdot cos(\phi)], \tag{3.9}$$

where P is the beam polarization, $\frac{d\sigma_0}{d\Omega}(\Theta)$ the unpolarized cross section, Θ the scattering angle in the laboratory frame, ϕ the azimuthal angle and A_y the analysing power. The scattering angle is measured from the outgoing beam direction and the azimuthal angle ϕ from the horizontal direction, see Fig.3.24.

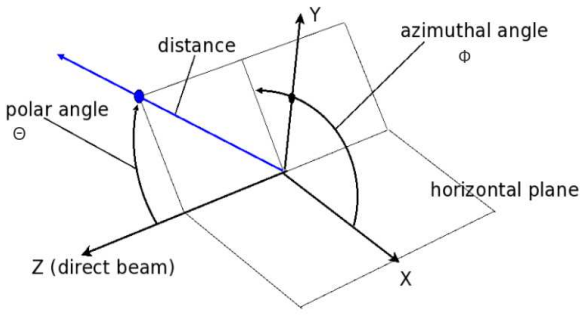

Figure 3.24: Scattering plane.

STEP 1: Beam polarization calculation

The first stage of the algorithm consists in the calculation of the beam polarization P. P is calcuted using the deuteron asymmetry of the *pd* elastic channel. The number of recorded counts in a detector

N(Θ,ϕ)[38] is:

$$N(\Theta,\phi)_{L,R} = n \cdot d_t \cdot \Delta t \cdot \Delta\Omega_{L,R} \cdot Eff_{L,R} \cdot \frac{d\sigma}{d\Omega} \tag{3.10}$$

Here n is the number of particles incident on the target, d_t is the target areal density, Δt is the measurement time, $\Delta\Omega_{L,R}$ is the solid angle covered by the left (L) and the right (R) detector, Eff$_{L,R}$ are the detector efficiencies and $\frac{d\sigma}{d\Omega}$ is the differential cross section defined in eqn.3.9. This count number is recorded for the left L ($\phi = 0$) and the right R ($\phi = \pi$) detectors and for runs with polarization state up and down ($\uparrow\downarrow$) resulting in the four quantities: $N_{L\uparrow}$,$N_{R\uparrow}$,$N_{L\downarrow}$,$N_{R\downarrow}$.
One can define the relation:

$$\delta = \sqrt{\frac{N_{L\uparrow} \cdot N_{R\downarrow}}{N_{L\downarrow} \cdot N_{R\uparrow}}} = \frac{1 + P \cdot A_y(\Theta)}{1 - P \cdot A_y(\Theta)} \tag{3.11}$$

where $\Delta\Omega$ and the integrated luminosity ($n \cdot d_t \cdot \Delta t$) cancel out. The detected asymmetry is defined as:

$$\epsilon = \frac{\delta - 1}{\delta + 1} = P \cdot A_y \tag{3.12}$$

Equation 3.12 is the cross-ratio method[39]. The cross-ratio allows the measurement of P in a way indepedent of relative detector efficiencies, of solid angles, of a target thickness variation and of the difference of the luminosities for up and down polarized beams at first order.
The error on ϵ is given by:

$$\Delta\epsilon = \frac{\sqrt{2 \cdot (N_{L\downarrow} \cdot N_{R\uparrow} \cdot N_{L\uparrow} \cdot N_{R\downarrow})}}{(\sqrt{N_{L\uparrow} \cdot N_{R\downarrow}} + \sqrt{N_{L\downarrow} \cdot N_{R\uparrow}})^2} \tag{3.13}$$

If one considers the dependence of the analysing power on the azimuthal angle, the Eqn.3.12 has to be corrected for the average of the azimuthal coverage of the detector and can be expressed by:

$$\epsilon = P \cdot A_y \cdot < cos\phi > \tag{3.14}$$

To measure the beam polarization P from equation 3.14, the pd elastic channel has been taken into account since its analysing power is known at 49.3 MeV[46]. The deuterons asymmetry has been considered (deuterons selection has been realized using the PID method, see Fig.3.10).

A fit to the original data points of A_y (pd elastic)[46], has been accomplished according to the parabola:

$$A_y(\theta) = a(\theta - \theta_0) \cdot [1 + b(\theta - \theta_0)] \tag{3.15}$$

where a,b,θ_0 are the fit parameter. The experimental original data with the fitted curve is reported in Fig.3.25. Combining equations 3.14 and

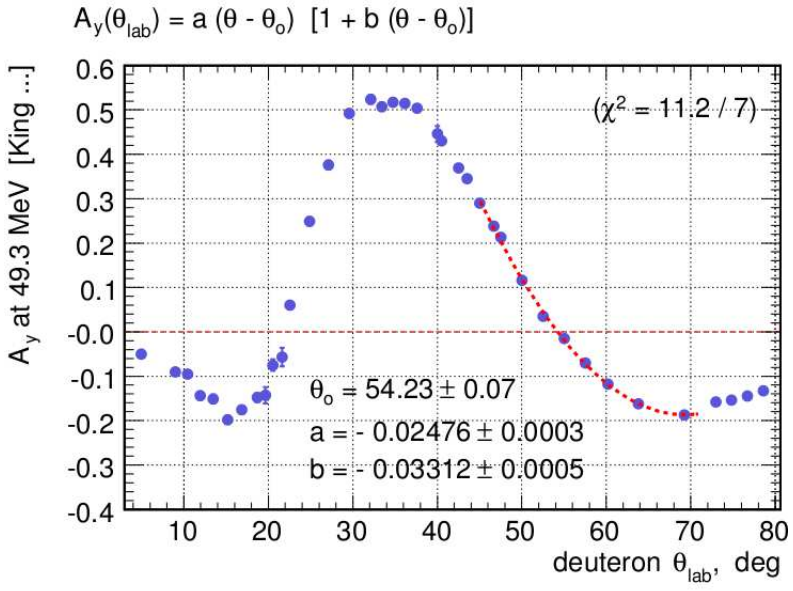

Figure 3.25: The experimental data vs the deuteron scattering angle θ_d from [46] fitted by the curve3.15. This figure taken from[41].

3.15 for pd elastic channel, the measured deuterons asymmetry ϵ can expressed by:

$$\epsilon = P \cdot A_y^{el} \cdot < cos\phi >= P \cdot a(\theta - \theta_0) \cdot [1 + b(\theta - \theta_0)] \cdot < cos\phi > \tag{3.16}$$

The beam polarization P has been measured by a χ^2 fit of the measured asymmetry, perfomed with MINUIT, using as a fit function the parabola of equation 3.16 where P is the only free parameter. The resulting weighted average of the beam polarization for the analysed runs has been determined to be:

$$P = 0.476 \pm 0.032 \tag{3.17}$$

The cross-ratio method employed to calculate the asymmetry cancels out any differences in luminosity, efficiency and acceptance of the

two detectors, so contibutions to systematics are excluded. In addition dead-time effects are negligible as the total system has a dead-time of < 100 μs and the count-rate was always well below 500/s.
A possible source of systematic uncertainty can be due to a fake asymmetry from moving beam target overlap that can cause a change of the beam-target overlap leading to a change of the measured asymmetry; nevertheless a systematic shift of the beam-target overlap between two different spin states, is identical to a different geometrical acceptance and cancels in first order by the used double ratio method and for this measurement can be ignored in systematics determination.

STEP 2: $\mathbf{A}_y$ calculation in *pd* breakup

Equation 3.14 can be specified for the neutron case and inverted to obtain A_y:

$$A_y = \frac{\epsilon_{NEU}}{P \cdot < cos\phi >}. \tag{3.18}$$

In this equation the beam polarization P is known from 3.17 and ϵ is the up/down asymmetry calculated with respect to the neutron according to:

$$\epsilon = \frac{UP - DOWN}{UP + DOWN}, \tag{3.19}$$

where UP refers to the number of identified neutrons when the polarization state is UP and DOWN is the number of identified neutrons when the polarization state is DOWN. The quantity $< cos\phi >$ is intergrated over the acceptance and taken to be equal 1.
As already pointed out in the previous sections, the pd→ppn Deuteron Breakup is a reaction involving three particles in the final state which can be kinematically described by 5 independent variables. These can be choosen among the jacobi momenta and angles: $\mathbf{p}$, $\mathbf{q}$, $\theta_{\mathbf{p}}$, $\phi_{\mathbf{p}}$, $\theta_{\mathbf{q}}$, $\phi_{\mathbf{q}}$, $\Delta\phi_{\mathbf{pq}}$ and the excitation energy E_{pp}, where in particular $\mathbf{q}$ represents the momentum of the neutron in the center of mass system.
The analysing power A_y of the reaction can be determined with respect to one of these variables and integrating over the others. Fot the current analysis, the measurement of the Analysing power of pd→ppn has been carried out as a function of Φ_q, as shown in Fig.3.26.

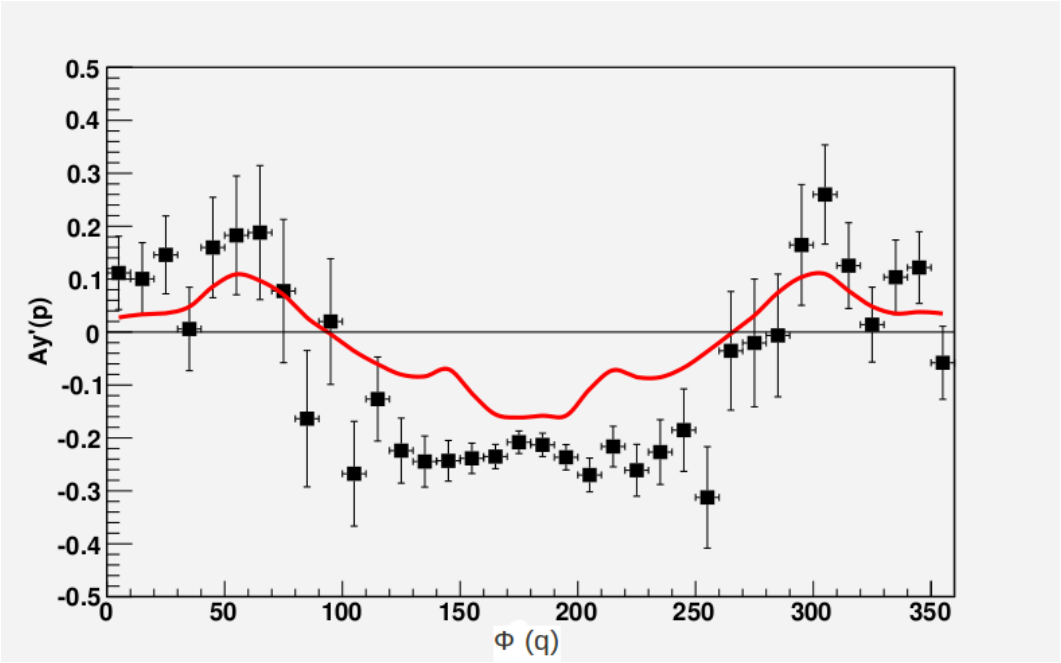

Figure 3.26: A_y of pd breakup calculated with respect to the neutron as a function of ϕ_q. For this plot all the identified pd breakup samples 2-1,2-2,3-1,3-2 have been employed. The black points are experimental data obtained by selecting θ_q between 0 and 150 degrees. The error bars include statistical uncertainties and the beam polarization uncertainties. The red line represents the theory prediction according N2LO including 3N forces. It is obtained using the sampling method on a grid provided by A. Nogga; the chiral EFT at the basis of the grids is developed by E. Epelbaum and coworkers. Figure by P.Thörngren.

3.7.1 Considerations

As shown in Fig.3.26, the trend of A_y for experimental data and theroretical prediction is qualitatively consistent. However the limited statistics of experimental data and the difficulty to control systematic uncertainties due to the not optimal experimental conditions, do not allow for a more quantitative comparison.
This plot shows the need of more statistical precision at very small and very large angles. This can be achieved using a detection system with a large azimuthal and longitudinal phase space coverage.
At present this analysis method is being applied on experimental data aquired at COSY during a beam time perfomed in September 2011, under improved experimental conditions.

Chapter 4

Future plans: Dedicated setup for *pd* Breakup studies

Exploiting the experience and the results obtained with experimental data described in the previuos sections, the PAX collaboration is planning to perform systematic studies of spin observables in *pd* Breakup by means of a dedicated setup.
The studies are foreseen in the energy range between 30 and 50 MeV at the PAX setup at COSY-ring. As pointed out in chapter 1, this is an energy range with scarce measurements available in literature and a complete data set of spin observables is required to fully investigate the role of the three-nucleon forces.
This section is dedicated to the description of the future experimental equipment suitable to measure *pd* Breakup spin observables, such as analysing powers and spin- correlation coefficients. When investigating spin-correlation coefficients, one needs to analyse the angular distribution of the scattered particles and to this aim it is necessary to employ a detector with a large azimuthal acceptance. The detector should also has a large coverage along the beam direction to be compatible with a high density target, which is realized using a storage cell.

4.1 PAX Experimental Setup

The *pd* Breakup setup[1] will be installed at the newly PAX low-β section and interaction point (PAX-IP) in the COSY-ring, and will employ the same experimental setup designed for the PAX *spin-filtering*

experiments at COSY[57][1].

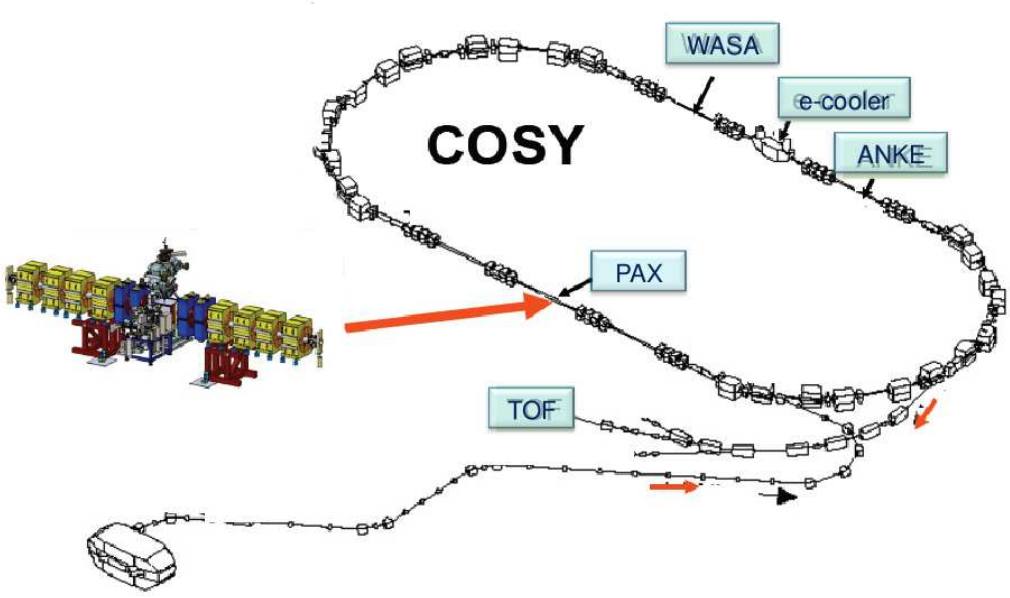

Figure 4.1: Layout of the COSY synchrotron accelator with the new low-β section, the ABS is placed above target chamber.

4.1.1 The COSY beam

In a cooled vertically polarized COSY beam, the maximum number of stored protons is $4 \cdot 10^9$ at 30 MeV and $5 \cdot 10^9$ at 45 MeV; with the electron cooler in operation these values are halved. In case of longitudinally polarized protons, injection losses caused by phase space couplings with the solenoid fields reduce the intensity to $6.7 \cdot 10^8$ at 30 MeV and $8.3 \cdot 10^8$ at 45 MeV. The clean identification of *pd*-elastic channel and the measured asymmetries at 30 MeV[43, 44, 45] and at 49 MeV[46, 47] used in the cross-ratio method[48] will provide the beam polarization. One of the required kinetic proton beam energy is 30 MeV. The beam has to be decelerated since the COSY injection energy is 45 MeV and the design of the ring is meant to operate at energies above 45 MeV, thus magnetic fields and power supplies are not designed for lower energies. Neverthless it is expected that the beam

[1]Some of the parameters that will follow in the description of the experimental setup are in fact constrained by spin-filtering requirements.

can be decelerated without a significative loss despite the reduced stability of the power supplies and reduced quality of the magnetic fields. During the deceleration phase, the adiabatic expansion of the beam being proportional to β_γ causes a beam loss of 20%; this loss can be smaller or even negligigle in case of cooled beam. In view of the proposed experiment, a commissioning of the cooling system and the PAX low β-section setting will be performed to test the possibility of having 30 MeV cooled beams in COSY.

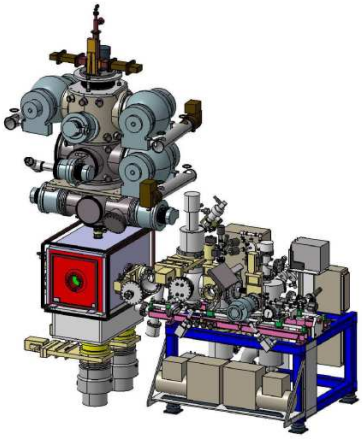

Figure 4.2: The PAX target section at COSY. The ABS is installed on the top of the target chamber. The proton beam passes through the target from behind. On the left side it is placed the BRP which is fed by small fraction of the beam extracted from the storage cell.

4.1.2 Polarized Internal Target

The PAX target is a polarized internal target (PIT) consisting of an atomic beam source (ABS)[54, 55] feeding a storage cell which is 40 cm long and has a diameter of 1 cm, and a Breit-Rabi polarimeter (BRP). The setup is shown in Fig.4.2.
Storage cells have been successfully employed at HERA (DESY)[50], at the TSR-ring (Heidelberg)[49], at Indiana University Cyclotron setup[51] and at ANKE-COSY[52, 53].
The use of a storage cell is requested to increase target density with respect to that of a free jet and allows to reach a luminosity in a range compatible with the experimental investigation. In particular, target densities up to 10^{14} atoms/cm^2 contibute to reach the required lumi-

nosity of about 10^{28} cm^{-2}s^{-1}. Hydrogen or Deuterium atoms in a single hyperfine-state are prepared in the ABS and injected into the storage cell. A small fraction of the target gas is extracted from the cell

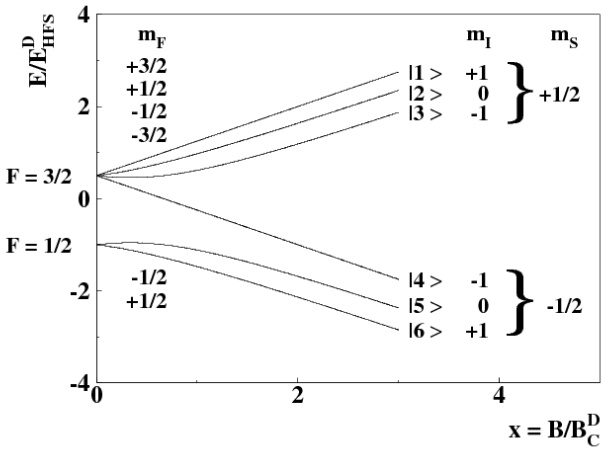

Figure 4.3: Breit Rabi diagram for deuterium. Energy eigenvalues for the hyperfine splitting of deuterium atom in an external magnetic field. E/E^D_{HFS} is the hyperfine splitting energy. B/B^D_c is the ratio between external field and the critical magnetic field of the deuterium, B^D_c=11.7 mT.

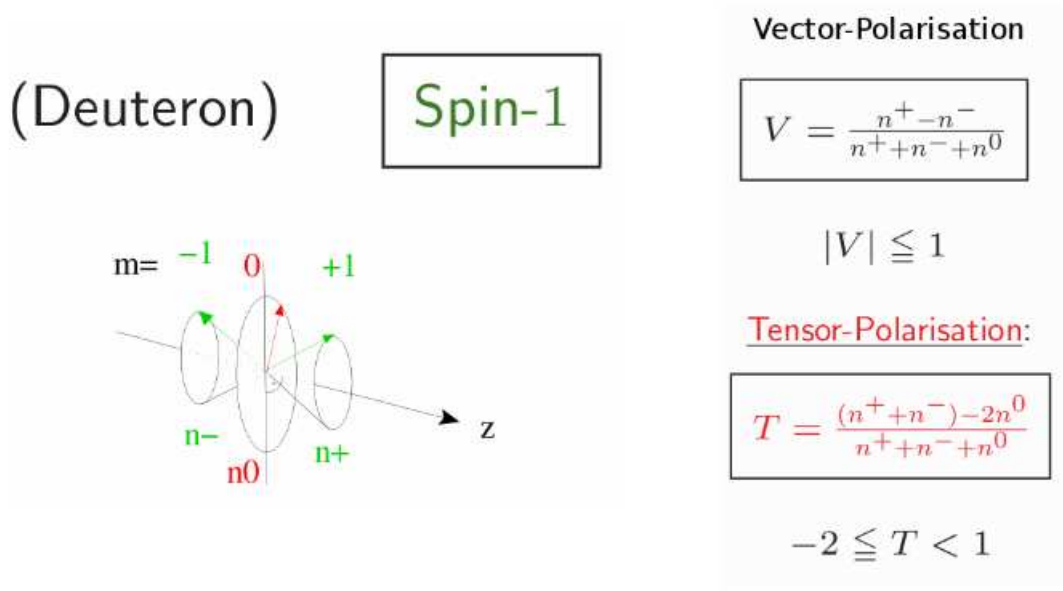

Figure 4.4: Figure taken from ref[56]

and enters the BRP where the atomic polarization measurement takes place. The sampled gas is also driven inside the Target Gas Analyzer (TGA) to determine the ratio of atoms to molecules in the gas.
The orientation of the quantisation axis for the atoms in the target along the horizontal (x), vertical (y), longitudinal (z) directions is defined by Helmholtz coils which create the weak magnetic holding fields of about 10 G surrounding the storage cell.
Both vector and tensor deuteron polarization will be necessary for the breakup experiment in order to have access to a larger number of spin observables.

4.2 PAX Multipurpose Detection System

To identify the *pd* Breakup reaction products, a dedicated detector design has been developing. This detector will be employed in spin-filtering experiments as well. This multipurpose detection system has to fulfill these requirements:

1. providing large acceptance along the cell to cover the 40 cm long interaction volume;

2. providing large azimuthal acceptance to allow spin correlation coefficients measurements;

3. working in vacuum to track low-momentum particles in the kinetic range from a few to a few tens of MeV;

4. measuring the spin dependent cross sections in *pd*, *pp* and $p\bar{p}$ elastic scatterings and to be used as polarimeter for the planned measurements at COSY and AD (CERN).

The detector consists of three layers of double-sided silicon strip sensors of large area ($99 \times 99\ mm^2$). The first two layers have a thickness of 300 μm. The third layer of 1.5 mm is introduced to increase the stopping power for the two outgoing protons and maximize the identification of *pd* Breakup events.
The system will be arranged in a up-down-left-right geometry rotated by 45 (barrel-like configuration) and will consist of 36 double-sided sensors (12 per quadrant). In each quadrant three layers are grouped

in three modules along the beam direction, as shown in Fig.4.5.

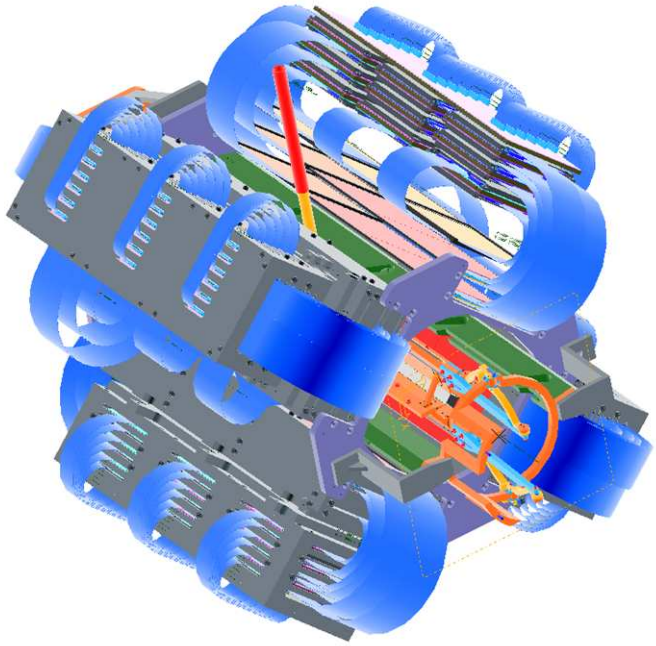

Figure 4.5: The PAX detector system. The silicon detectors (represented with kapton connection to the front-end electronics) surround the storage cell indicated in red is represented.

The strip pitch of 0.7 mm provides a vertex resolution of less than 1 mm. The 20 mm radial distance between silicon layers has been choosen to maximize azimuthal acceptance and to preserve the vertex resolution. See Appendix B for a description of the read-out electronics.
In the early design concept, the detection system consisted of the first two 300 μm layers solely. In order to maximize the identification of breakup events a third thicker layer is needed. At this aim I studied the possibility to add a third layer to cover the phase-space region where the maximum concentration of breakup events is expected. Two different thicknesses of the third layer have been implemented in simulations: 1 mm and 1.5 mm at two proton incident beam energies: 30 and 49 MeV. The results of this study are reported in a Letter of Intent[58] and have been published in [59]. The collaboration eventually decided to employ the 1.5 mm third layers since these are the only

available on the market for the required dimensions.

4.3 *pd* Breakup event generation

In the range 30-50 MeV a proton beam on deuteron target gives rise to *pd*-elastic and *pd* Breakup. Different samples of *pd*-elastic and *pd* Breakup Monte Carlo data have been investigated to tune the detector design to maximize the *pd* Breakup detection performance. The simulations tasks are:

- to optimize the detector geometry and positioning to maximize the geometrical acceptance and to minimize the uncertainties of measurement of kinematical variables;
- to estimate the expected detector performance depending on the kinetic proton beam energy (30,40 and 49 MeV) and on the impact of a third layer (1.5 mm).

For acceptance and event selection study the GENBOD event generator was employed. *GEANT* simulations were produced to study the detector response. The complete set of analysed Monte Carlo data is summarized in Table 4.1. The geometry implemented is shown in Fig.4.6.

Channel	T_p	3^{rd} **layer thickness**
pd-elastic 10^6 events pd-BUP 10^6 events	30 MeV	1.5 mm
pd-elastic 10^6 events pd-BUP 10^6 events	40 MeV	1.5 mm
pd-elastic 10^6 events pd-BUP 10^6 events	49 MeV	1.5 mm

Table 4.1: The first column indicates the simulated channels (10^6 events per channel), the second indicates the proton beam kinetic energy and the third column the thickness of the third layer.

4.4 *pd* Breakup events identification

The tracks reconsruction procedure is the same as described in Chapter 3. Depending on where the outgoing proton stops, one can

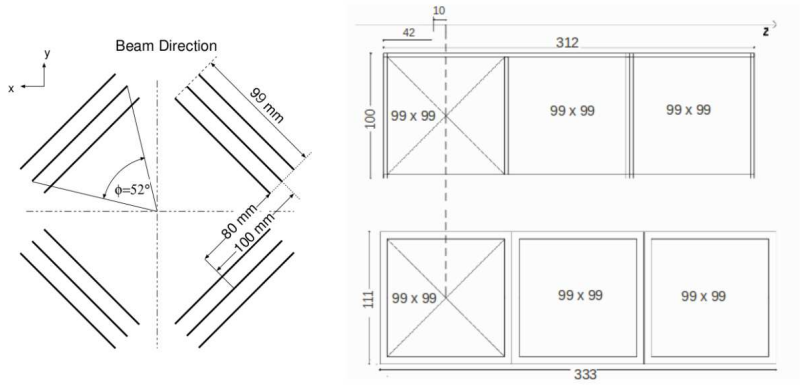

Figure 4.6: Schematic drawings of the detector setup front view (left) and side view of the first two layers (top right) and third layer (bottom right). Dimensions are expressed in mm. The dashed line represents the position of the detector along the z-axis respect to the target cell center. The thickenesses of the first two layers are 300 μm. The storage cell is 40 cm long made by 5 μm teflon.

select track "1", "2" or "3"; as a consequence the two outgoing protons give rise to 5 events samples 2-1, 2-2, 3-1, 3-2, 3-3 that are considered and studied separately. The first step to separate *pd*-elastic and *pd* Breakup is to exclude the overlap between *pd*-elastic and *pd* Breakup phace space loci using a co-planarity cut.

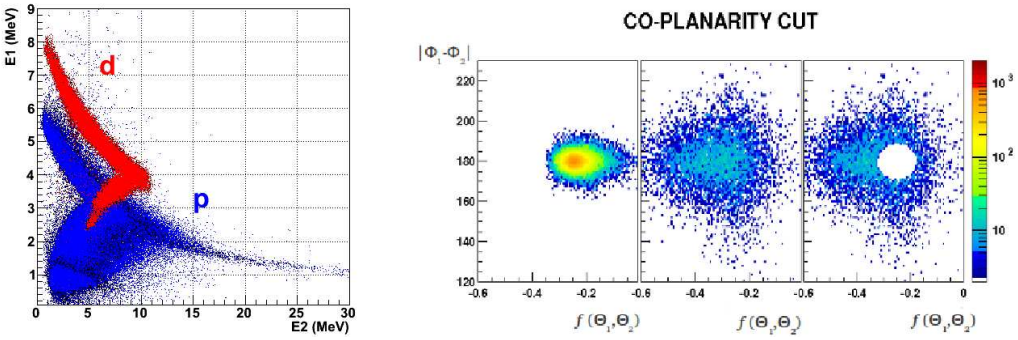

Figure 4.7: Monte Carlo: *pd*-elastic and *pd* Breakup events considered together. In the left panel the two channels are diplayed in the ΔE/E plot, the deuteron band is indicated in red, while the proton band in blue. To rule out *pd*-elastic, one asks for 2-track events in which both particles should belong to the proton loci and fullfill a co-planarity cut which exploits angular correlations between the scattered particles (right box). Right box: in the first panel only *pd*-elastic events are considered to evidence that they populate a well defined region of the phase-space; in the middle the *pd* Breakup phase space is shown. Breakup events populate a larger phase-space; in the left panel BreakUP phase-space in which the corresponding main concentration of *pd*-elastic has been excluded.

4.4.1 Stopped protons: track "1"

The candidate stopped protons in the first layer have to satisfy two conditions: first layer fired by one hit and the projection of the track must be inside the second layer acceptance, see Fig.4.8.

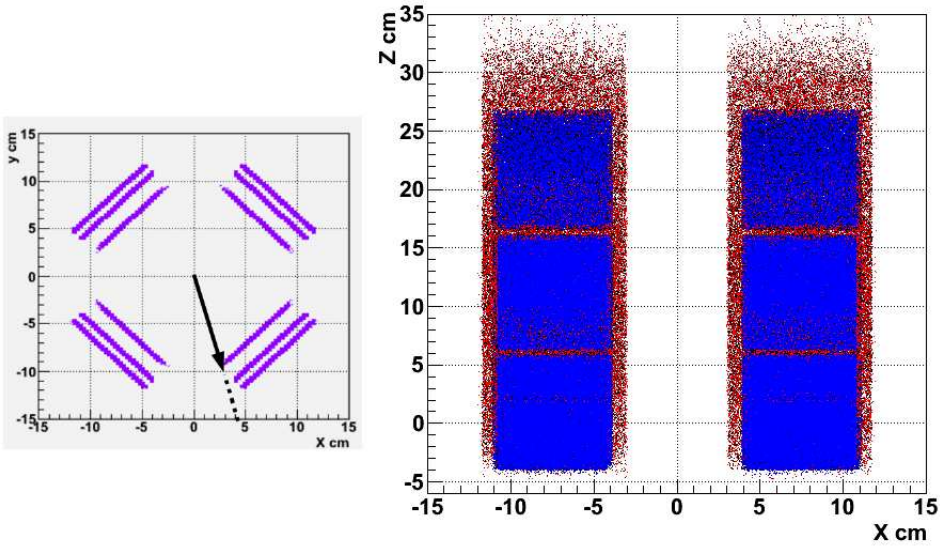

Figure 4.8: In the left panel the yx plane is shown. The black arrow indicates a particle that hits the first layer but misses the second layer acceptance so it is impossible to select it as stopped or not. The geometrical cut for track "1" is shown in the right panel. The blue points indicate the nominal position of the second layer, the red points are the projection of tracks with one hit in the first layer that miss the second layer acceptance. The ambiguity of one-hit tracks to be stopped or not is solved by requiring the projections to be inside the second layer acceptance.

4.4.2 Stopped protons: track "2" and "3"

Stopped protons in second (track "2") and third (track "3") layer are identified by a parametrization of the deposited energy. The selection criteria is presented for track "2", same procedure is applied for track "3".
In the $\Delta E/E$ plot, protons "truly" stopped in the second layer layer are identified by requiring that reconstructed and generated energies coincide, in Fig.4.9 they are highlighted in cyan. The region in red evidences the overlapping between stopped and no stopped protons. To allow the selection of stopped protons, the following procedure is used:

Step 1:

The "truly" stopped protons populate a curve that it is fitted by an hyperbola:

$$y = \frac{a}{x+b} \tag{4.1}$$

y is the energy deposited into the first layer E_1 and x is the deposited energy into the second layer E_2. The values of free parameters a and b enter the function:

$$f(E_1, E_2) = \frac{\frac{E_1}{a}}{E_2 + b} \tag{4.2}$$

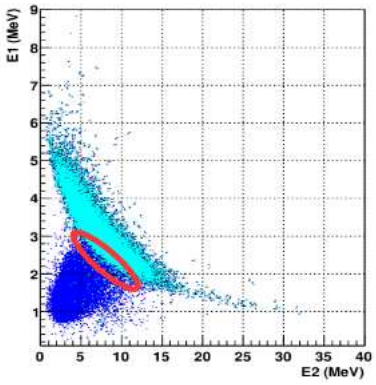

Figure 4.9: *pd* Breakup channel: Energy deposited in first layer E_1 versus energy deposited in second layer E_2. In Blue are represented protons that enter the second layer acceptance after passing the first layer. In Cyan are indicated "truly" stopped protons. The red curve shows the region where stopped and no stopped protons overlap.

Step 2:

The correlation $\frac{\frac{E_1}{a}}{E_2+b} vs E_2$ is represented in a scattered plot, see Fig.4.10. With this parametrization, a linear cut can be applied (magenta line) to separate the loci in which stopped and no stopped protons are mixed.

The same parametrization is applied to E_2 (energy deposited in the second layer) and E_3 (energy deposited in the third layer) to select particles stopped in the third layer. The result of this parametrization f(E_2,E_3) is shown in Fig.4.11.

Finally an efficiency/contamination study is carried out to optimize these selections.

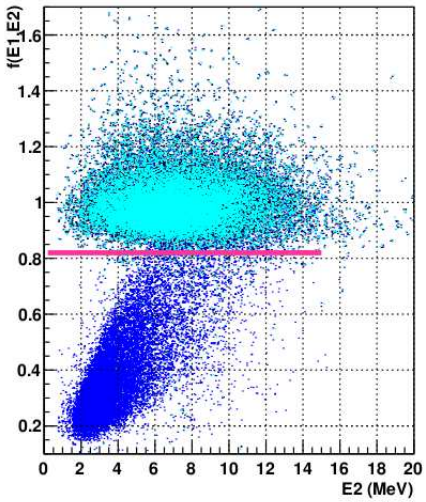

Figure 4.10: $\frac{\frac{E_1}{a}}{E_2+b} vs E_2$. In this plot it easier to select the expected stopped protons (in cyan) with respect to the no stopped ones (in blue) applying a linear cut (magenta line).

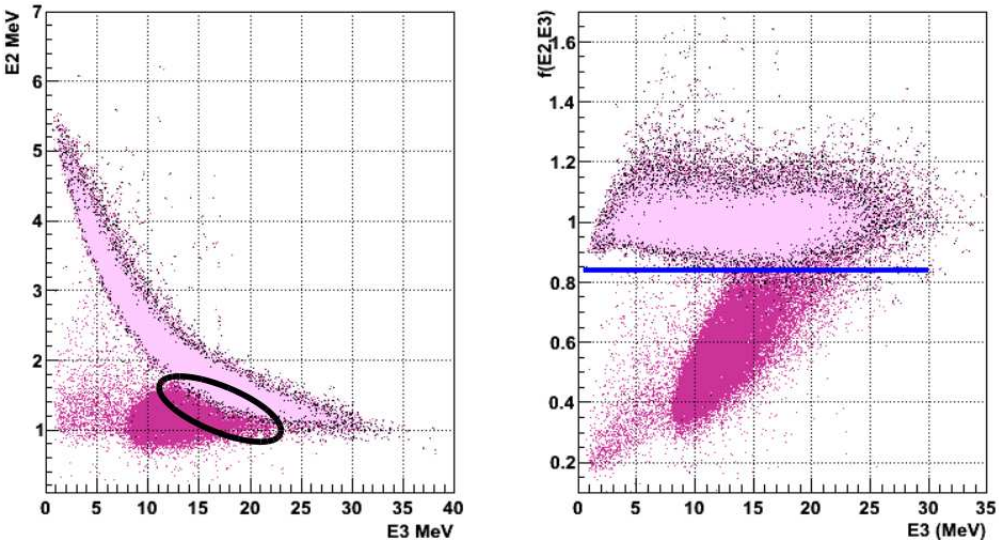

Figure 4.11: The energy parametrization to select stopped protons in the 3^{rd} layer is shown. In the left panel the ΔE/E plot is shown for particles entering the third layer: in light pink are indicated protons "truly" stopped in third layer. In black the overlap region of stopped and no stopped protons is indicated. In the right panel the parametrized energy plot is shown. The selection of stopped protons is realized with a linear cut (blue line).

4.5 *pd* Breakup reconstruction efficiency

The selection criteria have been worked out for the different Monte Carlo data sets. The five *pd* Breakup event samples have been identified

for each beam energy using these selection criteria and the Missing Mass has been calculated; an example of the Missing Mass spectra at 30 MeV is displayed in Fig.4.12. The number of entries for each spectra is used for estimating the expected reconstruction efficiency, whose results are shown in Table 4.4.

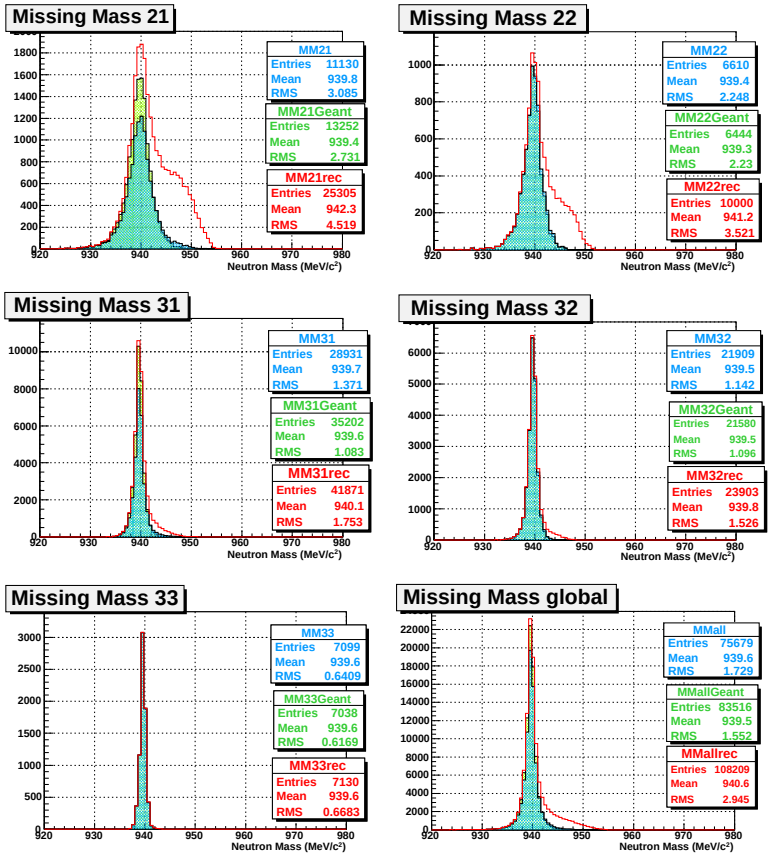

Figure 4.12: The Missing Mass distribution is shown for all event samples individually and together (bottom right panel). In each panel the Missing Mass distribution is displayed for (i) reconstructed events (selected events not necessary stopped) in red, (ii) for "truly" stopped events (selected events in which generated and reconstructed energy coincide) in green, (iii) for stopped events (events satisfying the selection criteria) in blue. The number of entries for each distribution is reported in the boxes next to the Missing Mass spectra.

4.6 Phase space coverage

To study the three-nucleon continuum is mandatory to have a large coverage of the phase-space.
The individual study of the Breakup samples 2-1, 2-2, 3-1, 3-2, 3-3 gives access to different regions of the phase-space. As an example, the jacobi momenta of samples 2-1 and 3-2 are shown for 30 MeV and 49 MeV proton beam kinetic energy.

- JACOBI MOMENTA at Tp=30 MeV

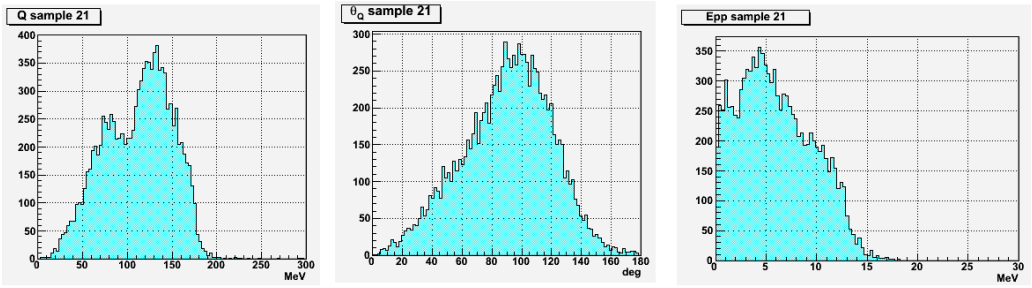

Figure 4.13: Sample 2-1 at Tp=30MeV: the left panel shows q, the momentum of the neutron in the centre of mass system, in the middle θq is displayed, in the right panel the excitation energy of the two outgoing protons is shown. Low excitation energies correspond to the case when the two scattered protons hit the same detector.

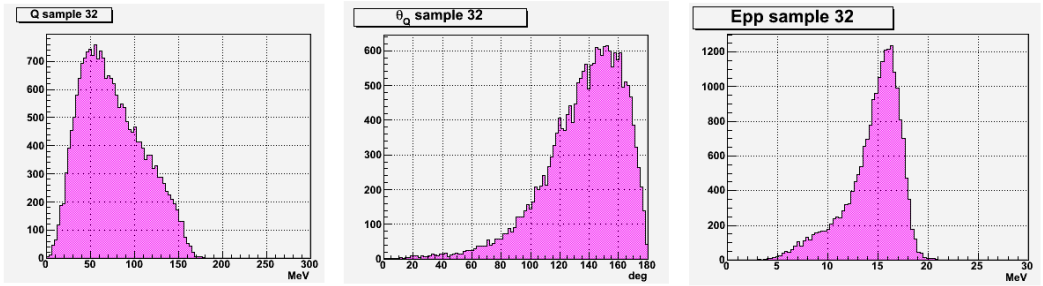

Figure 4.14: Sample 3-2 at Tp=30MeV: the left panel shows q, the momentum of the neutron in the centre of mass system, in the middle θq is displayed, in the right panel the excitation energy of the two outgoing protons is shown. In this sample the two scattered protons are more energetic with respect to the 2-1 case and the case when tracks are emitted in a symmetric configuration is privileged. As a consequence the excitation energy of the two scattered protons peaks at higher values with respect to the 2-1 case.

- JACOBI MOMENTA at Tp=49 MeV

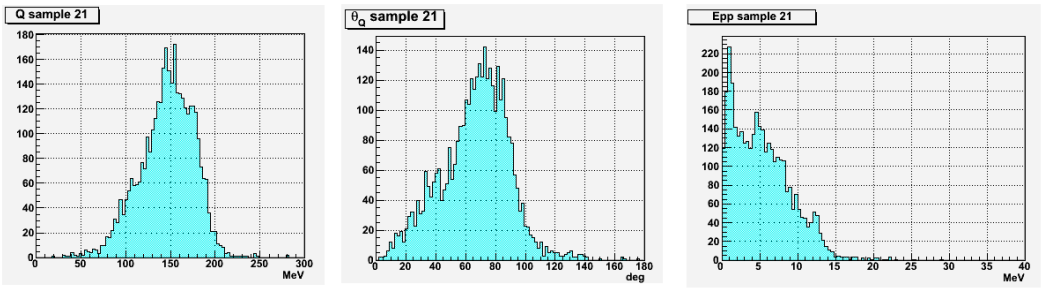

Figure 4.15: Sample 2-1 at Tp=49MeV: the left panel displays q, the momentum of the neutron in the centre of mass system, in the middle θq is represented, in the right panel the excitation energy of the two outgoing protons is shown.

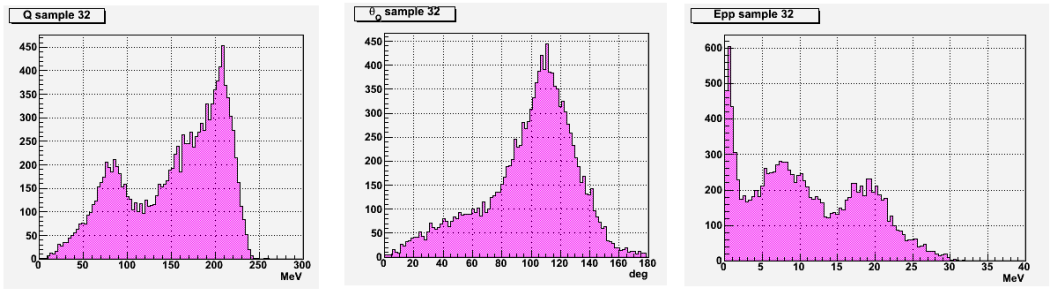

Figure 4.16: Sample 3-2 at Tp=49MeV: the left panel shows q, the momentum of the neutron in the centre of mass system, in the middle θq is displayed, in the right panel the excitation energy of the two outgoing protons is shown.

STATISTICS AT Tp=30 MeV			
SAMPLE	**RECONSTRUCTED**	**TRULY STOPPED**	**STOPPED**
21	25235	13241	11130
22	99567	6435	6610
31	41702	35069	28931
32	23732	21432	21909
33	7048	6956	7099
ALL	107684 (11%)	83133 (8%)	75679 (8%)

Table 4.2: Statistics for reconstructed events, GEANT "truly" stopped events and stopped by selection criteria events for 30 MeV is reported. The last row refers to the sum of all breakup samples. Left brackets: percentage of reconstructed events with respect to the total number of breakup events that enter the detector acceptance; middle: percentage of "truly stopped" events with respect to the total number of breakup events that enter the detector acceptance; right: percentage of stopped events using the selection criteria with respect to the total number of breakup events that enter the detector acceptance. The impact of the third layer increases by a factor 3 the stopping efficiency with respect to the case in which solely the first two layers are taken into account.

STATISTICS AT Tp=40 MeV			
SAMPLE	**RECONSTRUCTED**	**GEANT STOPPED**	**STOPPED**
21	22522	6464	5789
22	9905	4817	4633
31	57160	29432	24456
32	32326	18828	18399
33	25528	22843	21254
ALL	147441 (15%)	82384 (8%)	74516 (7%)

Table 4.3: Statistics for reconstructed events, GEANT "truly" stopped events and stopped by selection criteria events for 40 MeV is reported. The last row refers to the sum of all breakup samples. Left brackets: percentage of reconstructed events with respect to the total number of breakup events that enter the detector acceptance; middle: percentage of "truly stopped" events with respect to the total number of breakup events that enter the detector acceptance; right: percentage of stopped events using the selection criteria with respect to the total number of breakup events that enter the detector acceptance. The presence of the third layer increases by a factor 6 the stopping efficiency with respect to the case in which solely the first two layers are taken into account.

STATISTICS AT Tp=49 MeV			
SAMPLE	**RECONSTRUCTED**	**TRULY STOPPED**	**STOPPED**
21	20045	3739	3617
22	8112	2701	2674
31	64194	18739	16544
32	36063	13146	12942
33	40141	16784	16236
ALL	168555 (17%)	55109 (6%)	52013 (5%)

Table 4.4: Statistics for reconstructed events, GEANT "truly" stopped events and stopped by selection criteria events for 49 MeV is reported. The last row refers to the sum of all breakup samples. Left brackets: percentage of reconstructed events with respect to the total number of breakup events that enter the detector acceptance; middle: percentage of "truly stopped" events with respect to the total number of breakup events that enter the detector acceptance; right: percentage of stopped events using the selection criteria with respect to the total number of breakup events that enter the detector acceptance. The impact of the third layer increases by a factor 7 the stopping efficiency with respect to the case in which solely the first two layers are taken into account.

4.6.1 Considerations

The analysis chain developed for the *pd* breakup events identification has been successfully applied to a sample of Monte Carlo data in which the new dedicated detection system configuration has been implemented. This analsyis has been carried out at three different proton beam kinetic energies. The stopping efficiency calcuted with respect to the total number of generated events within the detector acceptance is 8% at Tp=30 MeV, 7% at Tp=40 MeV and 5% at Tp=49 MeV. The impact of the third layer of 1.5 mm thickness increases the stopping efficiency with respect to the case in which solely the first two layers are considered, by a factor 3 at Tp=30 MeV, by a factor 6 at Tp=40 MeV and by factor 7 at Tp=49 MeV.

Conclusions

The present work has been dedicated to the study of the *pd* Breakup reaction. The study constitutes a part of a project persued at the COSY storage ring. This project is finalized to map pd breakup spin observables in a kinematical region where measurements are scarce altough strongly needed to fix important constraints for extending the present knowledge of the three-nucleon forces via the Chiral Perturbation Theory.

In the first part of the work, I developed an analysis chain to investigate whether a detection system based on Silicon Tracking Telescope, originally conceived to identify *pd* elastic events, was capable to identify the products of the *pd* Breakup reaction. This feasibility study has been successfully applied to an existing data sample taken at the COSY ring in Febrauary 2008, with a vertically polarized proton beam of 49.3 MeV kinetic energy impinging on a Deuterium cluster target. In a following phase, the identified *pd* Breakup events have been employed to tune an algorithm to measure the analysing power in *pd* Breakup reaction using the neutron asymmetries. This observable represents one of the probes to constrain Chiral Perturbation Theory. The analysis of the available data sample has allowed to outline the experimental conditions required for an exhaustive investigation of the spin observables in *pd* breakup reaction. On the other side, the low statistics and the not optimal working conditions of the detection system made not possible to finalize the result on the existing data sample. At present the developed analysis is being adopted on a new sample of data acquired during 2011 beam-time, under better experimental conditions.

In parallel, I carried out a study of a new apparatus esplicitly dedicated to the *pd* Breakup investigation. In particular double spin asym-

metries in *pd* Breakup offer a rich laboratory where testing Chiral Perturbation Theory. An ideal enviroment for accessing these observables would be an experiment where both the proton beam and the deuterium target are polarized. In addition a detection system providing a large azimuthal and longitudinal phase-space coverage would be needed.
For this reason, I implemented the analysis software for the characterization and the optimization of this dedicated detection system on Monte Carlo generated data. This detection system is simmetrically arranged around the interaction point equipped with the storage cell to increase the density of the polarized target and consists of 12 telescopes.36 silicon detectors, 9 per quadrant (3 layers of 3 adjacent modules). In detail, I investigated the optimization of the geometry along the beam direction and the impact of an additional thicker layer to maximize the stopping efficiency. This study shows that the detection system equipped by a the third layer of 1.5 mm thickness, increases the stopping efficiency, with respect to the case in which solely the first two layers are employed, up to a factor 7 at Tp=49 MeV. The results of the analysis have been included in a proposal[1] submitted and successfully reviewed from the PAC of COSY.

Appendix A

A systematic approach to the three-particle phase space : The Sampling Method

This section is dedicated to the description of the *Sampling Method*, see ref.[60], a technique developed for the analysis of the breakup observables; this method will be used and further developed for the investigation of pd breakup observables for the foreseen experiment at COSY.
The *pd* breakup observables analysis has been limited by the constraint that the comparison to theory was commonly performed over a restricted phase space region, the S-curve, defined as the kinematically allowed region in the plane of the two detected nucleons[61].
This restriction is overcome making use of the *Sampling Method*[2], which is a tool developed to fully exploit the large coverage of phase space by detection systems and make use of a kinematically complete knowledge of the final state of the reactions. This method can be applied to any final state populated by three particles. This method can provide the theoretical prediction of a specific observable once the complete kinematical information of an event is determined. To realize a complete kinematical description of a three-particle final state, one needs five parameters, that can be choosen to be: p,θ_p,ϕ_p,θ_q,ϕ_q, being the momenta p and q defined as:

$$p = \frac{1}{2}(p_1 - p_2) \tag{3}$$

$$q = -(p_1 + p_2) \tag{4}$$

[2]Original idea by Prof.H.O.Meyer, developed by P. Thörgren Engblom and J.Kuroś-Zołnierczuk

p_1 and p_2 are the momenta of the two outgoing protons calculated in the center mass system and satisfying the condition $p_1 > p_2$, therefore the polar angle belong to the range [0,90] degrees; q is the momentum of the neutron, and the corrispective polar and azimuthal angle are $\theta_{p(q)}$ and $\phi_{p(q)}$.

The calculation of an observable entails the selection of the indepen-

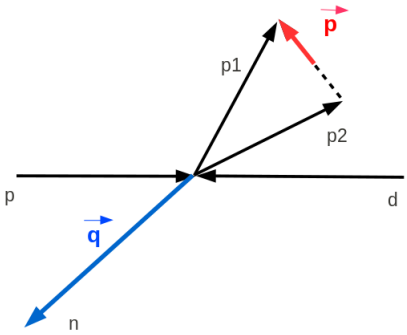

Figure 17: Jacobi momenta of $pd \to ppn$ in the center-of-mass system. p=1/2(p1+p2) and q=-(p1+p2)

dent variable to be used and the selection of the phase spac1e region to integrate over.

One has to know precisely the acceptance and any efficiency variation, which can be achieved using dedicated Monte Carlo simulations.

A given set of experimental data (γ), containing the phase space points, is used as the input to a theoretical model calculation that can be compared to the theory by taking the mean of the predicted values:

$$O^{th} = \frac{\Sigma O^{th}(x_i)}{N(\gamma)} =< O^{th} >, \tag{5}$$

with $N(\gamma)$ the total number of events. The statistical error of the theoretical prediction deriving from the randomness of the sampling is givem by the standard deviation.

The comparison between calculations with and without 3NF included gives the sensitivity of a specific observable.

The sampling method has been implemented for the analysis of axial observables[64] and tensor analyzing powers[65] in dp-breakup at E_N = 135 MeV.

The sampling method using a grid is used in planning experiments and in handling with complex data analysis.

Spin Observables

This section is devoted to the description of the spin formalism, refering to G.G.Ohlsen, in the most general expression for correlation parameters of the spin dependent cross section for spin 1/2 and spin 1, together with the vector and tensor moments, taking into consideration the terms violating parity in elastic scattering. In the traditional coordinate system used, the beam is along the z-axis, the y-axis is taken positive upwards and the x-axis sideways is fixed in order to complete a right-handed coordinated system, following the Madison convention[67].
Concerning the notation fo the observables and the spin alignment: the vector and tensor analyzing powers are A_i and $A_{jk,}$, where i,j,k = x,y,z respectively; the vector correlation parameters are C_{ij}, the tensor vector correlation parameters are $C_{ik,j}$ (the first index ik refers to the deuteron polarization, the second j refers to the proton polarization); the proton vector moments are indicated with $p_{x,y,z}$, while the deuteron vector components are $q_{x,y,z}$ and the tensor moments are q_{jk} (j,k = x,y,z).
The polarized cross section σ, being σ_0 the unpolarized part, is defined by:

$$
\begin{aligned}
\sigma \;=\; & \sigma_0(1 + p_y A_y(p) + p_z A_z(p) + \frac{3}{2} q_y A_y(d) + \frac{3}{2} q_z A_z(d) \\
& + \frac{3}{4}(q_x p_x + q_y p_y)(C_{x,x} + C_{y,y}) + \frac{3}{4}(q_x p_x - q_y p_y)(C_{x,x} - C_{y,y}) \\
& + \frac{3}{4}(q_y p_x - q_x p_y)(C_{y,x} - C_{x,y}) + \frac{3}{2} q_x p_z C_{x,z} + \frac{3}{2} q_z p_x \; C_{z,x} + \frac{3}{2} q_z p_z C_{z,z} \\
& + \frac{1}{6}(q_{xx} - q_{yy})(A_{xx} - A_{yy}) + \frac{1}{2} q_{zz} A_{zz} + \frac{2}{3} q_{xz} A_{xz} \\
& + \frac{1}{6}(q_{xx} - q_{yy}) p_y (C_{xx,y} - C_{yy,y}) + \frac{1}{2} q_{zz} p_z C_{zz,z} + \frac{1}{2} q_{zz} p_y C zz, y \\
& + \frac{2}{3} q_{xy} p_x C_{xy,x} + \frac{2}{3} q_{xz} p_y C_{xz,y} + \frac{2}{3} q_{yz} p_x C_{yz,x} \\
& + \frac{2}{3} q_{xy} p_z C_{xy,z} + \frac{2}{3} q_{yz} p_z C_{yz,z} + \frac{1}{3}(q_{xz} p_x + q_{yz} p_y)(C_{xz,x} + C_{yz,y}))
\end{aligned}
$$

Vector and Tensor moments

Concerning the notation to define the vector and tensor moments: the absolute polarization of the proton is indicated with P and the vector (tensor) polarization of the deuteron with Q (Qt); ϕ_p and β_p are respectively the azimuthal and the polar angles of the proton spin alignment, ϕ_d and β_d in case of the deuteron spin alignment.
The vector moments of the proton spin are given by:

$$p_x = Psin(\beta_P)cos(\Phi_P - \phi) \tag{6}$$

$$p_y = Psin(\beta_P)sin(\Phi_P - \phi) \tag{7}$$

$$p_z = Pcos(\beta_P) \tag{8}$$

The vector moments of the deuteron spin are given by:

$$q_x = Qsin(\beta_Q)cos(\Phi_Q - \phi) \tag{9}$$

$$q_y = Qsin(\beta_Q)sin(\Phi_Q - \phi) \tag{10}$$

$$q_z = Qcos(\beta_Q) \tag{11}$$

The six tensor moments of the deuteron polarization are defined as:

$$q_{xx} = \frac{1}{2}Qt(3(sin(\beta_d))^2(cos(\Phi_d - \phi))^2 - 1) \tag{12}$$

$$q_{yy} = \frac{1}{2}Qt(3(sin(\beta_d))^2(sin(\Phi_d - \phi))^2 - 1) \tag{13}$$

$$q_{zz} = \frac{1}{2}Qt(3(cos(\beta_d))^2 - 1) \tag{14}$$

$$q_{xy} = \frac{3}{2}Qt(sin(\beta_d))^2 sin(\Phi_d - \phi)cos(\Phi_d - \phi) \tag{15}$$

$$q_{yz} = \frac{3}{2}Qtsin(\beta_d)cos(\beta_d)cos(\Phi_d - \phi) \tag{16}$$

$$q_{yz} = \frac{3}{2}Qtsin(\beta_d)cos(\beta_d)sin(\Phi_d - \phi) \tag{17}$$

Polarization Observables and Theoretical Predictions

The polarized cross section and the vector-tensor moments can be linked to a specific spin observable once the particular configuration of the beam-target have been fixed expliciting the value of the polarization alignments of the beam and target particles in equations defining σ and the moments.
In this section some predictions are shown for the foreseen measurements of pd-breakup with E_N=30-50 MeV. The independent observables (7 analysing powers and 15 spin correlation coefficients) that can be accessed via proton deuteron breakup are listed in fig.18 together with the required combination of spin alignment of the proton beam and deuterium target for each observable.
Theoretical grids based on chiral EFT and N2LO for vector and tensor analysing powers and correlation coefficients have been created to identify regions in phase space sensitive to 3N effects; the theoretical predictions are functions of the jacobi momenta. The input for the sampling is generated isotropically in a phase space simulation; multidimensional linear interpolation is applied to retrieve the theoretical prediction for each event.

PolObs	pU dU	pU dS	pU dA	pA dU	pA dS	pA dA	pU dAU	pU dAS
$A_y(p)$	X	X	X				X	X
$\mathbf{A_z(p)}$				X	X	X	pA dAU	pA dAS
$A_y(d)$	X	X		X	X		X	X
$\mathbf{A_z(d)}$			X			X	X	X
$A_{xx} - A_{yy}$	X	X		X	X		X	X
A_{zz}	X	X	X	X	X	X	X	X
A_{xz}							X	X
$C_{x,x} + C_{y,y}$	X						X	
$C_{x,x} - C_{y,y}$	X	X					X	X
$\mathbf{C_{y,x} - C_{x,y}}$		X						X
$C_{x,z}$				X	X		pA dAU	pA dAS
$C_{z,x}$			X				X	X
$C_{z,z}$						X	pA dAU	pA dAS
$C_{xx,y} - C_{yy,y}$	X	X					X	X
$\mathbf{C_{xz,x} + C_{yz,y}}$						X	X	
$\mathbf{C_{zz,z}}$				X	X	X	pA dAU	pA dAS
$C_{zz,y}$	X	X	X				X	X
$C_{xy,x}$	X	X					X	X
$C_{xz,y}$							X	X
$C_{yz,x}$							X	X
$C_{xy,z}$				X	X		pA dAU	pA dAS
$C_{yz,z}$							pA dAU	pA dAS

Figure 18: Summarized here are the 15 spin observables and 7 analysing powers possible in proton deuteron breakup showing the required polarization alignment directions of beam and target and some combinations thereof. For p (proton) and d (deuteron); Umeans alignment up (vertical), S is sideways (parallell to the x-axis) and A is along the beam direction (longitudinal).The last two columns refer to the situation when the deuteron spin alignment axis is at 45 degrees which can be accomplished by running current through two guide field coils simultaneously. With the longitudinal ($\pm$ z) and vertical ($\pm$ y) guide field coils on, denoted dAU, and switched in $\pm$ polarity, four directions are achieved. Another four alignments are obtained with the longitudinal and sideways ($\pm$ x) combinations, denoted dAS. There are five observables (here marked in bold font) that are parity forbidden in elastic scattering and goes to zero in breakup reactions in coplanar kinematical configurations. In the last two columns also a few observables are included requiring longitudinally polarized beam. The tensor-vector correlation coefficient $C_{yz,z}$ is accessible only using longitudinally polarized beam and diagonal target spin alignment.

Appendix B

Read-out electronics for PAX multipurpose detector

The read-out electronics for the PAX detector is based on the one developed for the ANKE detector. The in-vacuum board carries the read-out chips with 11 MeV linear range, time resolution better than 1 ns and able to provide a fast signal for triggering. The power supplies, control signals, trigger pattern threshold and calibration pulse amplitudes to the front-end chips are provided by the interface card outside vacuum. The vertex board (developed in Juelich) comprises a sequencer together with a 12 bit ADC with 10 Mhz sampling; it allows common-mode correction for hardware zero-suppression regime to minimize the output flow to 0.1 MByte per second with a dead time less than 50μs. Since the dynamic range increases with increasing deposited energies by protons, some modifications of the chips of the thicker layer are required for allowing the detection the outgoing stopping protons. The analysis of Monte Carlo concerning the energy loss in the thicker layer, allowed to define the expected maximum deposited energy by protons and thus to define the required dynamic range of the chips.

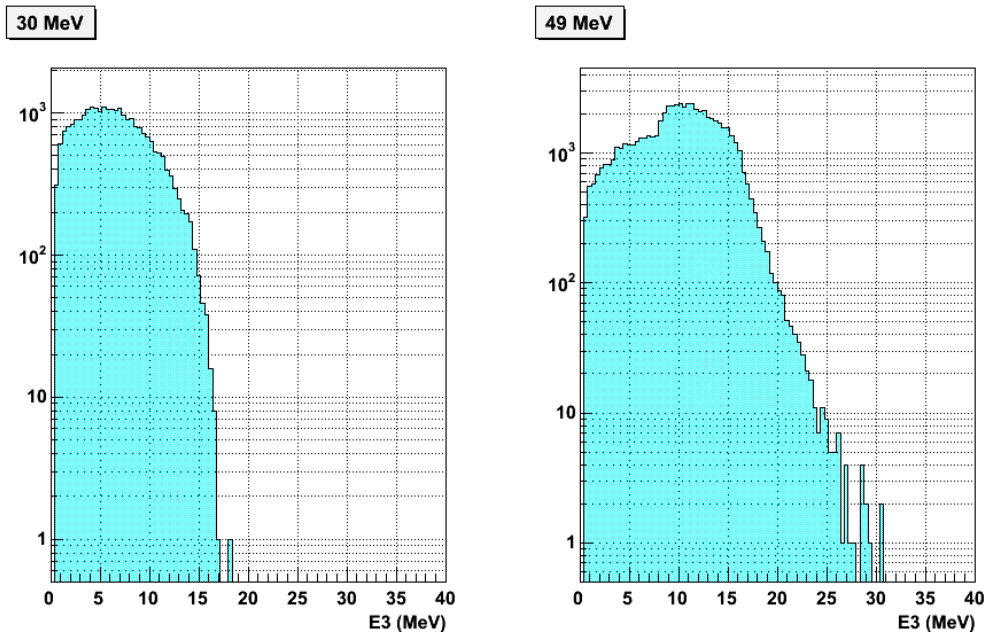

Figure 19: Monte Carlo: deposited energies by protons in 1.5 mm detector at 30 MeV proton beam kinetic energy (left panel) and 49 MeV (right panel) after passing through the first two layers of 300 μm displayed in log scale. The maximum value of the deposited energy, see x-axis, is 17 MeV at proton beam Tp=30 MeV and 30 MeV at proton beam Tp=49 MeV.

Bibliography

[1] P. Thörngren Engblom et al., Measurement of Spin Observables in the $\vec{p}\vec{d}$ Breakup Reaction COSY Proposal 202.1 (2011), submitted to the COSY Program Advisory Committee by the PAX collaboration, www2.fz-juelich.de/ikp/publications/PAC39/PAX_proposal202.1_202.pdf

[2] H. Primakoff and T. Holstein, Phys. Rev. 55 (1939) 1218.

[3] N. Kalantar-Nayestanaki, E. Epelbaum, J.G. Messchendorp and A. Nogga, Signatures of three-nucleon interactions in few-nucleon systems, Rep. Prog. Phys. 75 (2012) 016301.

[4] E. Epelbaum, H.-W. Hammer, Ulf-G. MeiÃ§ner, Modern Theory of Nuclear Forces, arXiv:0811.1338v1 [nucl-th] 2008.

[5] H. Yukawa, Proc. Phys. Math. Soc. Jap. 17, 48 (1935).

[6] R. B. Wiringa, V. G. J. Stoks, and R. Schiavilla, Phys. Rev. C 51, 38 (1995).

[7] R. Machleidt, K. Holinde, and Ch. Elster, Phys. Rep. 149, 1 (1987)

[8] R. Machleidt, Adv. Nucl. Phys. 19, 189 (1989)

[9] R. Machleidt, Phys. Rev. C 63, 024001 (2001).

[10] V. G. J. Stoks, R. A. M. Klomp, C. P. F. Terheggen, and J. J. de Swart, Phys. Rev. C 49, 2950 (1994).

[11] Tornow W, WitaÅĆa H and Kievsky A 1998 Phys. Rev. C 57 555

[12] S. C. Pieper and R. B. Wiringa, Ann. Rev. Nucl. Part. Sci. 51, 53 (2001).

[13] J. Fujita and H. Miyazawa, Prog. Theor. Phys. 17, 360 (1957).

[14] B.v. Przewoski *et al.*, [arXiv: nucl-ex/0411019], Phys. Rev. C 74 (2006) 064003

[15] K. Sekiguchi *et al.*, Phys. Rev. C 70 (2004) 014001

[16] S. Kistryn *et al.*, Phys. Rev. C 72, 044006 (2005).

[17] S.Weinberg, Physica A96 (1979) 327.

[18] U. van Kolck, Phys. Rev. C49 (1994) 2932; E. Epelbaum et al., Phys. Rev. C66 (2002) 064001.

[19] P.F. Bedaque and U. van Kolck, Ann. Rev. Nucl. Part. Sci. 52 (2002) 339; E. Epelbaum, Prog. Part. Nucl. Phys. 57 (2006) 654.

[20] A. Nogga, P. Navratil, B. R. Barrett and J. P. Vary,Phys. Rev. C 73, 064002 (2006).

[21] E. Epelbaum, A. Nogga, W. Glökle, H. Kamada, G. MeiÃ§ner and H. Witala, Phys. Rev. C 66, 064001(2002).

[22] P. Navratil, V. G. Gueorguiev, J. P. Vary, W. E. Ormand and A. Nogga, Phys. Rev. Lett. 99, 042501(2007).

[23] R. Maier, Nucl. Instrum. Meth. A390, 1 (1997).

[24] H. Dombrowski et al., Nucl. Instrum. Meth. A 386, 228 (1997).

[25] Micron Semiconductor Ltd. http://www.micronsemiconductor.co.uk.

[26] D. Boutigny *et al.*, BaBar Technical Design Report. Technical report, SLAC-R-95- 457 Report, March 1995.

[27] C.Bozzi *et al.*, The design and construction of the BaBar silicon vertex tracker. Nucl. Instr. and Meth. in Phys. Res., A447:15-15, 2000.

[28] C.Bozzi *et al.*, The BaBar Silicon Vertex Tracker. Nucl. Instr. and Meth. in Phys. Res., A461:162-167,2001.

[29] G.Batignani *et al.*, Geometrical Specifications of the Silicon Detectors Barrel Detectors, BaBar Not #284, March 29, 1996.

[30] G.Batignani *et al.*, Specifications and Quality Control Procedures of Silicon Detectors for SVT, BaBar Not #312, July 12, 1996.

[31] D. Protic, T. Krings, and R. Schleichert, IEEE Trans. Nucl. Sci. 49, 1993 (2002).

[32] Oellers D. *et al.*,Polarizing a stored proton beam by spin flip? PLB 674 (2009) 269-275

[33] S.N. Bunker et al., Nucl. Phys., A113 (1968) 461, N.S.P. King it et al., PL, 69B (1977) 151

[34] wwwads.web.cern.ch/wwwasd/geant/index.html

[35] V. Hejny et al. A new analysis framework for ANKE. www2.fz-juelich.de/ikp/publications/AR2002/CHAP1/1120.pdf

[36] Oellers D. et al., Spin-Filtering Studies at COSY (Beam request), http://www2.fz-juelich.de/ikp/pax/portal/index.php?id=404

[37] P.Lenisa,F.Rathmann, Summary of the August to October 2011 PAX beam-time at COSY, http://www2.fz-juelich.de/ikp/pax/portal/index.php?id=406

[38] G. Ohlsen and P. Keaton, Nucl. Instrum. Meth. 109, 41 (1973).

[39] R. Hanna, Proceedings of the 2nd Int. Symp. on Polarization Phenomena of Nucleons, Karlsruhe, Germany, 1965.

[40] N.S.P. King et. al., Phys. Lett 69B, 2 (1977).

[41] Gogi Macharasvili: '$p_{\uparrow}$d $\rightarrow$ pd analysis(EXP_181) Pax Feb-2008 beam time'.

[42] D.Oellers, *Polarizing a Stored Proton Beam by Spin-Flip?* PhD thesis, Universität Köln, 2010.

[43] S. J. Hall, A. R. Johnston and R. J. Griffiths, Phys. Lett., 14, 212-214 (1965).

[44] A.R. Johnston et al., Phys. Lett. 19, 289-291, (1965).

[45] H. Dobiasch, et al., Phys. Lett. B 76, 195-196 (1978).

[46] N.S. King et al., Phys. Lett. B 69, 151 (1997).

[47] A.R. Johnston et al., Phys. Lett. 21, 309-311 (1966).

[48] R.C. Hanna, Proceedings of the 2nd International Symposium on Polarization Phe- nomena 1965, Karlsruhe, Birkhaeuser, Basel, p. 280 (1966).

[49] K. Zapfe et al., Rev. Sci. Instrum. 66, 28 (1995).

[50] A. Airapetian et al., Nucl. Instrum. Methods A 540, 68 (2005).

[51] T. Rinckel et al., Nucl. Instrum. Methods A 439, 117 (2000).

[52] A. Kacharava, F. Rathmann, and C. Wilkin for the ANKE Collaboration, COSY Proposal #152, Spin Physics from COSY to FAIR; available from http://www2.fz-juelich.de/ikp/anke.

[53] K. Grigoryev et al., Proc. of the 17th Int. Spin Physics Symp., Kyoto, Japan, 2006, Eds. K. Imai, T. Murakami, N. Saito, and K. Tanida, AIP Conf. Proc. 915 (AIP, Melville, NY, 2007), p. 979.

[54] A. Nass et al., Nucl. Instrum. Meth. A 505, 633 (2003)

[55] T. Wise, A.D. Roberts, W. Haeberli, Nucl. Instrum. Methods A 336, 410 (1992).

[56] C.Riedl, Die Messung der Tensor-Strukturfunktionen bd. 1 und bd. 2 mit dem Hermes-Experiment, www-hermes.desy.de/.../criedl.dpgtp2003.pdf

[57] D.Oellers, C.Weidemann et al. COSY Proposal *Spin-Filtering Studies at COSY* http://www2.fz-juelich.de/ikp/pax/portal/index.php?id=404

[58] Letter of Intent submitted to the COSY Program advisory Committee by the PAX collaboration *Measuremet of Spin Observables in the pd Breakup reaction*, available from: www.fz-juelich.de/ikp/pax, Spokespersons of the proposal Thorngren Engblom P. September 2009.

[59] S.Bertelli *Deuteron-breakup reaction studies at COSY* Nuovo Cimento C, Volume 034, Issue 05, pp 29-34.

[60] J. Kuros-Zolnierczuk, P. Thörngren Engblom, H.O. Meyer, T.J. Whitaker, H. Witala, J. Golak, H. Kamada, A. Nogga, R. Skibinksi, Few Body Syst. 34, 259- 273 (2004).

[61] G. G.Ohlsen, Nucl. Inst. Meth. 179, 283 (1981)

[62] J. Kuroś-Zołnierczuk et al., Phys. Rev. C 66, 024003 (2002).

[63] J. Kuroś-Zołnierczuk et al., Phys. Rev. C 66, 024004 (2002).

[64] H.-O. Meyer et al., Phys. Rev. Lett. vol. 93 no 11, (2004) 112502

[65] P. Thörngren Engblom et al., The 19th European Few-Body Conference, Groningen Aug. 23-27, 2004, [arXiv: nucl-ex:0410006], AIP Conf. Proc. 768, 65-68 (2005)

[66] E. Epelbaum, W. Glöckle and U.-G. MeiÃ§ner, Nucl. Phys. A 747, 362 (2005).

[67] Madison Convention, Proceedings International Conference on Polarization Phenomena in Nuclear Reactions, Madison 1971, p.XXV, S.E.Darden, p.39.

Acknowledgements

I would like to thank all the people who shared with me these three years.
Desidero ringraziare il mio tutor, Dr. Paolo Lenisa per avermi dato l'opportunità di portare avanti il mio progetto di tesi, per la pazienza, il prezioso supporto e la fiducia. Ringrazio il Dottor Marco Contalbrigo per i suggerimenti riguardo l'analisi dati e ringrazio il Dottor Giuseppe Ciullo per i chiarimenti e le discussioni in materia di Fisica e Didattica. Ringrazio la Prof.ssa Paola Ferretti per i consigli e la sua disponibilità. Un gran grazie particolare lo dedico al Dr. Luciano Pappalardo per il suo preziosissimo aiuto.
I would like to thank Pia Thörngren for her constant guidance, her support and advices throughout these years. I would like to thank Mirian Tabidze and Gogi Macharashvili for providing me data and for their avalaibility for explanations and advices for the analysis.

Infine ringrazio tutta la mia famiglia.